

EXTENDED OPTICAL LINE EMITTING GAS IN POWERFUL RADIO GALAXIES: STATISTICAL PROPERTIES AND PHYSICAL CONDITIONS

STEFI A. BAUM¹

Netherlands Foundation for Radio Astronomy, National Radio Astronomy Observatory,² and
 University of Maryland

AND

TIMOTHY HECKMAN¹

University of Maryland

Received 1988 February 12; accepted 1988 June 21

ABSTRACT

In this paper, we present the statistical results of a search for extended optical emission-line gas in a sample of 38, predominantly "powerful," flux-density selected, radio galaxies (the "representative sample") and of an additional five radio galaxies. We have obtained optical broad-band and narrow-band and VLA radio images of these sources (Baum *et al.*).

We establish that spatially extended emission-line gas is common in powerful radio galaxies. We detect line emission from all of the sources in the representative sample. In ~85% of these sources we have spatially resolved the line emission. The median extent of the emission-line nebulae is 10 kpc, and the median emission-line luminosity in H α + [N II] or [O III] is 3×10^{41} ergs s⁻¹, roughly an order of magnitude times the extent and luminosity of emission-line nebulae found in normal elliptical galaxies of similar optical magnitude. The median extent of the emission-line nebulae in sources with low radio luminosities ($L_{\text{radio}} < 10^{42.7}$ ergs s⁻¹) or edge-dimmed (Fanaroff and Riley Class I) radio morphologies is roughly one-fourth the median extent of the nebulae in the higher power sources.

We estimate lower limits to the density of the emission-line gas at distances between 5 and 10 kpc from the galaxy nucleus of 0.1-1 cm⁻³, and upper limits to the total mass in emission-line gas between 5×10^7 and $5 \times 10^9 M_{\odot}$.

We find that the narrow emission-line luminosity is strongly correlated with both the total radio luminosity and the radio core power in the sources from the representative sample, and that the core radio power is strongly correlated with the total radio luminosity.

The number of photons required to photoionize the emission-line nebula is found to correlate strongly with the number of ionizing photons emitted by the galaxy nucleus, as estimated from measurements of the nuclear, "nonstellar" continuum from the host galaxy. These results, combined with the spectroscopic and modelling, results of Robinson *et al.*, suggest that photoionization by the host galaxy's nuclear ultraviolet continuum is the dominant means by which both the nuclear and the extended emission-line gas in powerful radio galaxies is ionized. The strong correlation of Q_{nuc} with Q_{tot} suggests that the emission-line luminosities are limited by the flux of ionizing photons emitted by the active nucleus rather than by the availability of hydrogen atoms.

We consider possible origins for the emission-line gas. Instabilities in the hot intergalactic medium of the host galaxy may be the source of the emission-line gas in sources which have small (i.e., kiloparsec scale) emission-line nebulae. However, the large spatial extent of the emission-line nebulae in some very isolated galaxies and the possible large associated masses in emission-line gas may suggest that these very extensive regions of emission-line gas did not originate in the ISM. For sources with very extended regions of emission-line gas which inhabit densely populated regions, the emission-line gas may, however, have cooled out of a hot intergalactic medium. We also consider the possibility that the emission-line gas in these galaxies originates in tidal interactions/mergers with companion galaxies which are rich in cold gas. In support of this possibility, we find that the median extent of the emission-line nebulae is larger in galaxies which show possible signs of a recent interaction than in either dumbbell galaxies or galaxies which show no signs of a recent interaction.

We show that there are roughly two orders of magnitude in radio luminosity separating the luminosity regime in which the sources in our sample have exclusively edge-darkened (Fanaroff and Riley [1974] Class I) radio morphologies from the regime where sources have exclusively edge-brightened or hotspot (Fanaroff and Riley, Class II) radio morphologies. We find a tendency for the radio source axis to align with the minor axis of the host radio galaxy only in galaxies which have radio sources which are greater than 200 kpc in extent. Roughly 25% of the sources in the representative sample show obvious morphological peculiarities in the distribution of their continuum optical isophotes.

Subject headings: galaxies: clustering — galaxies: interactions — galaxies: nuclei — galaxies: structure —
 radio sources: extended — radio sources: galaxies

¹ Visiting Astronomer Kitt Peak National Observatory, operated by AURA, Inc., under contract to the National Science Foundation.

² The National Radio Astronomy Observatory is operated by Associated Universities Inc., under contract with the National Science Foundation.

I. INTRODUCTION

This is the second in a series of papers discussing extended optical emission-line gas in radio galaxies. We have obtained optical broad-band (R or V) and narrow-band (isolating redshifted $H\alpha + [N II]$, or $[O III]$) images of a representative, radio flux density selected, sample of 38 radio galaxies (hereafter the “representative sample”) and of an additional five radio galaxies which we knew to be interesting from prior observations (hereafter the “special” sample). We also obtained VLA radio images of most of the sources in the sample at ($1''$ – $10''$ resolution). In Baum *et al.* (1988; hereafter Paper I) we described the sample selection, the observations, and the data reduction, presented contour maps of the optical broad-band, emission-line and VLA radio images, and discussed, in detail, the characteristics of the individual sources. The reader is encouraged to refer to Paper I prior to reading this article.

We note that the radio sources in the representative sample were selected primarily on the basis of their radio flux density at a low frequency (408 MHz) and are (with one exception) extended radio sources with steep spectral indices ($\alpha < -0.5$, for $f_\nu \propto \nu^\alpha$). The sources span a wide range in radio luminosity from only 2×10^{40} ergs s^{-1} to 2×10^{45} ergs s^{-1} .³ However, 31 of the 38 sources in the representative sample and four of the five sources in the special sample have radio luminosities greater than 10^{42} ergs s^{-1} (or equivalently powers at 1.4 GHz, $P_{1.4} \gtrsim 10^{24.5} h_0^{-2}$ ergs s^{-1} Hz $^{-1}$, where $h_0 = H_0/100$). In this sense, the great majority of the sources in our sample are “powerful” radio galaxies.

In this paper, we will concentrate on the global results for the sample as a whole, rather than on peculiarities found in individual sources. The statistical results and the conclusions drawn from them are based only on the observations of the “representative sample.” In §§ IIa–IIc, we present the radio, broad-band optical, and emission-line results, respectively. In § II d, we investigate correlations between the radio, broad-band optical, and emission-line properties of the sources. In § II e, we calculate limits to the density and mass in the extended emission-line gas. In § III a, we discuss the confinement of the extended emission-line gas. In § III b, we present evidence which suggests that nuclear photoionization is the dominant means by which both the nuclear and the extended emission-line gas is ionized. In § III c, we consider possible origins for the emission-line gas. Finally, in § IV, we summarize the results and review their implications.

II. RESULTS

a) Radio Imaging

i) Radio Source Parameters

In Table 1, we list parameters of the radio source structures. From our VLA radio images and published radio images we have extracted, for each source, the core flux density and position, the total extent of the source, the position angle of the orientation of the large-scale radio structure, and the bending angle of the radio source in the sources with hotspots at the ends of their radio source structure. We note that the concept of radio source extent, although clearly defined for sources with well-defined edges (i.e., sources with terminal hotspots), is ambiguous for sources in which the radio emission fades gradually with distance from the nucleus. For these sources, we

have taken the source extent to be the maximum distance spanned by the lowest significant radio isophote. We have utilized our radio images as well as lower resolution images from the literature; in all cases at least 90% of the total source flux density, as determined from single-dish measurements, was represented on the radio image used.

The radio source position angle was determined as follows. For the radio sources having a hotspot in each lobe, the position angle was taken to be the mean of the position angle defined by each of the hotspots and the core. For the sources lacking hotspots, the position angle was taken to be the orientation of emission seen nearest to the nucleus. The radio source bending angle is defined as 180° minus the angle defined by lines connecting each hotspot with the core. We also list the total source flux density at 408 MHz, the spectral index, and the total radio luminosity calculated assuming high- and low-frequency cutoffs of 10^{11} and 10^7 Hz, respectively, a Hubble constant (H_0) of $75 \text{ km s}^{-1} \text{ Mpc}^{-1}$, and a deceleration parameter (q_0) of 0.0.

ii) Classification of Radio Source Structure

We classify each source in terms of its radio morphology after Fanaroff and Riley, 1974 (see col. [2] of Table 1). Fanaroff and Riley defined as Class I (hereafter FR1) those sources in which the ratio of the distance between the regions of highest surface brightness on opposite sides of the central galaxy or quasars to the total source extent is less than 0.5. Class II sources (hereafter FR2), then, are those in which this ratio is greater than 0.5. FR1 radio sources typically show relatively smoothly declining radio brightness with distance from the nucleus, while FR2 sources show emission which terminates in bright hotspots. The classification of radio source structure in this way can clearly be dependent on the resolution with which the source is imaged, the frequency at which the source is imaged, and the angle from which we observe the source.

In our sample, we find several sources that do not share the radio morphologies typically seen in sources which are classified as having FR1 or FR2 radio structures. Two sources from our special sample, 3C 171 and 3C 305, have bright *interior* hotspots close to the galaxy nucleus and larger, diffuse trails of radio emission extending laterally from the hotspots, perpendicular to the inner jet axis. Thus these sources exhibit the hotspots characteristic of FR2 sources, but the edges of the sources are characterized by diffuse radio emission, as in FR1 sources. We have labeled the source structure seen in these two sources as FR2_{dstb}, to indicate the disturbed, atypical nature of their radio morphologies. One additional source from our sample (3C 433) has a very unusual radio morphology. This source has a resolved, weak hotspot in only one lobe which has a very steep outer intensity gradient, and only diffuse (if any) radio emission associated with the opposing lobe. We term the radio morphology of this source “FR2?.” There are other sources in our sample which satisfy the technical criteria for FR2 sources, but in which one or both of the hotspots (perhaps better described as warm spots) are weak and resolved. For the purpose of this paper, since these sources do undisputedly terminate in brightness enhancements, we classify the morphologies of these “transition” sources as FR2.

We also note two sources in our sample (PKS 0745–191 and 3C 196.1) which have amorphous radio structures. Specifically, there is no clear morphological evidence in either of these sources (either direct or indirect) for a collimated outflow from the galaxy nucleus. In both cases the radio emission is asym-

³ Throughout this paper we assume a Hubble constant (H_0) of 75 km s^{-1} and a deceleration parameter (q_0) of 0.0.

TABLE 1
RADIO RESULTS

Source	Type	S ₄₀₈	α	S _{core}	L _{radio}	P _{core}	size''	size kpc	PA	ΔPA
3C 29 *	2	10.74	-0.6	0.042 ^a	3.8 × 10 ⁴²	1.6 × 10 ³⁰	138	112	160	4
3C 33 *	2	31.79	-0.7	0.034	1.5 × 10 ⁴³	2.3 × 10 ³⁰	265	281	19	4
3C 40 *	1	14.60	-0.9	0.04 ^f	3.8 × 10 ⁴¹	2.4 × 10 ²⁹	1200	396	10	...
B2 0149 + 358	1	0.36 ^g	-1.2	0.007 ^a	6.6 × 10 ³⁹	3.4 × 10 ²⁸	52	16	66	...
3C 63 *	2	11.06	-0.8	0.016	3.8 × 10 ⁴³	9.4 × 10 ³⁰	22	59	34	8
3C 75N *	1	15.35	-0.8	0.039 ^g	9.0 × 10 ⁴¹	4.7 × 10 ²⁹	240	108	120	...
3C 75S *	1	...	-0.8	0.018 ^g	...	1.9 × 10 ²⁹	240	108	148	...
3C 78 *	1	14.18	-0.5	0.7	2.9 × 10 ⁴²	1.1 × 10 ³¹	177	95	49	...
3C 88 *	2	10.31	-0.6	0.168 ^d	1.7 × 10 ⁴²	2.9 × 10 ³⁰	226	127	58	4
3C 89 *	1	10.63	-1.0	0.041	1.7 × 10 ⁴³	1.5 × 10 ³¹	60	133	115	...
PKS 0349-278 *	2	12.03	-0.8	0.015	5.5 × 10 ⁴²	1.3 × 10 ³⁰	241	281	55	2
3C 98 *	2	25.99	-0.7	0.0075	3.2 × 10 ⁴²	1.3 × 10 ²⁹	311	177	26	8
3C 105 *	2	11.06	-0.6	0.0137	1.6 × 10 ⁴³	2.1 × 10 ³⁰	335	508	129	7
3C 109 *	2	11.06	-0.8	0.219 ^b	1.3 × 10 ⁴⁴	4.0 × 10 ³²	96	386	145	13
PKS 0634-206 *	2	22.55	-0.8	0.0145	7.3 × 10 ⁴²	8.7 × 10 ²⁹	870	872	179	1
3C 171	2 _{dstb}	8.40 ^e	-0.84	0.002 ^h	5.3 × 10 ⁴³	2.2 × 10 ³⁰	10	34	99	4
PKS 0745-191 *	AM	9.85	-1.05	0.18	8.0 × 10 ⁴²	3.5 × 10 ³¹	11	19	155	...
3C 192 *	2	11.02 ^f	-0.8	0.008 ⁱ	4.1 × 10 ⁴²	5.5 × 10 ²⁹	192	204	124	2
3C 196.1 *	AM	8.20 ^f	-0.73	0.06	4.3 × 10 ⁴³	4.5 × 10 ³¹	8	23	42	...
3C 218 *	1	117.70	-0.9	0.217	3.0 × 10 ⁴³	1.2 × 10 ³¹	80 (240)	79 (237)	5	6
3C 219 *	2	21.60 ^d	-0.8	0.005 ^j	7.8 × 10 ⁴³	2.9 × 10 ³⁰	184	491	40	0
3C 223 *	2	8.00 ^a	-0.75	<0.003 ^e	1.9 × 10 ⁴³	<1.1 × 10 ³⁰	300	659	164	3
3C 227 *	2	20.84	-0.8	0.020	1.6 × 10 ⁴³	2.8 × 10 ³⁰	227	336	86	10
3C 264 *	1	18.26	-1.0	0.260	5.9 × 10 ⁴¹	2.2 × 10 ³⁰	50 (540)	20 (215)	30	...
3C 272.1 *	1	13.32	-0.6	0.186 ^k	2.2 × 10 ⁴⁰	3.4 × 10 ²⁸	150	9	175	...
3C 274 *	1	548.17	-0.8	2.1 ^l	6.3 × 10 ⁴¹	4.6 × 10 ²⁹	840	55	112	...
3C 275 *	2	10.20	-0.9	...	2.8 × 10 ⁴⁴	...	6	32	50	0
3C 278 *	1	15.68	-0.6	0.076 ^d	5.7 × 10 ⁴¹	3.1 × 10 ²⁹	165	46	177	...
3C 285	2	5.00 ^d	-0.62	0.008 ^m	5.4 × 10 ⁴²	9.1 × 10 ²⁹	182	252	81	19
PKS 1345+125 *	core	8.27	-0.4	...	4.5 × 10 ⁴³	...	< 0.1	< 0.2
3C 295 *	2	49.50 ^a	-0.63	0.0095 ^c	2.2 × 10 ⁴⁵	4.0 × 10 ³¹	5	27	143	2
3C 305	2 _{dstb}	9.60 ^e	-1.0	0.008 ⁿ	1.2 × 10 ⁴²	2.6 × 10 ²⁹	13	10	45	9
3C 313 *	2	10.85	-0.9	<0.001	2.7 × 10 ⁴⁴	<4.2 × 10 ³⁰	130	671	59	2
3C 317 *	1	24.92	-1.2	0.232 ^b	2.2 × 10 ⁴²	5.4 × 10 ³⁰	65	42	5	...
3C 321	2	8.20 ^a	-0.6	0.032 ^a	1.4 × 10 ⁴³	5.7 × 10 ³⁰	300	488	136	1
3C 327 *	2	21.80	-0.9	0.037	2.1 × 10 ⁴³	7.7 × 10 ³⁰	169	294	100	2
3C 327.1 *	2	14.40 ^e	-1.02	0.065	3.3 × 10 ⁴⁴	2.8 × 10 ³²	19	98	119	23
3C 346 *	2	9.77	-0.8	0.249	2.8 × 10 ⁴³	1.2 × 10 ³²	13	33	71	0
3C 353 *	2	122.97	-0.7	0.137 ^b	1.5 × 10 ⁴³	2.4 × 10 ³⁰	265	150	83	14
3C 390.3 *	2	34.30 ^d	-1.1	0.35 ^o	7.8 × 10 ⁴²	2.1 × 10 ³¹	212	213	144	0
3C 403 *	2	14.61	-0.9	0.0098	4.4 × 10 ⁴²	6.5 × 10 ²⁹	212	213	87	12
3C 405 *	2	4400.00 ^d	-0.7	0.327 ^p	1.8 × 10 ⁴⁵	2.0 × 10 ³¹	124	125	113	0
3C 433 *	2?	27.54	-0.7	0.005	3.9 × 10 ⁴³	9.9 × 10 ²⁹	63	108	166	...
3C 442 *	2	12.35	-1.0	0.0034 ^d	6.4 × 10 ⁴¹	4.5 × 10 ²⁸	524	257	47	12

Col. (1):—Source name. An asterisk denotes membership in the complete sample.

Col. (2):—Morphological classification of radio source structure (e.g., Fanaroff and Riley 1974). See text for more details.

Col. (3):—Total source flux density in janskys at 408 MHz, on the Baars *et al.* 1977 flux scale. Unless otherwise noted fluxes are taken from the Parkes catalog (Staff of the Division of Radiophysics, CSIRO 1969). Superscripts give the reference for the 408 MHz flux, as follows: *a*, interpolated from the 178 MHz flux and spectral index between 750 and 38 MHz as given by Spinrad *et al.* 1985; *b*, Greuff and Vigotti 1973; *c*, taken from Molongio results (Large *et al.* 1981); *d*, McDonald, Kenderdine, and Neville 1968; *e*, Elsmore and Mackay 1969; *f*, interpolated from the 635 MHz Parkes flux and a spectral index of -0.73 between 635 and 960 MHz as given by Wills 1975; *g*, Colla *et al.* 1973. 3C 75 is actually comprised of two radio sources, but the flux of the individual sources cannot be separated. Therefore we list the combined source flux at 408 MHz of 3C 75, under the entry for 3C 75N.

Col. (4):—Spectral index between 408 and 1400 MHz, except for 3C 192 which is between 408 and 5000 MHz, unless otherwise noted in the notes to col. (3). References as for col. (3).

Col. (5):—Core radio flux, as measured from our 6 cm VLA B-array maps, unless otherwise noted. Superscripts as follows: *a*, core flux at 21 cm from A-array VLA map; *b*, core flux at 2 cm from C-array VLA map; *c*, core flux at 2 cm from A-array VLA map; *d*, core flux at 6 cm from a C-array VLA map; *e*, core flux at 20 cm from a B-array VLA map; *f*, C. O'Dea, private communication 1987; *g*, F. Owen, private communication 1987; *h*, Heckman, van Breugel, and Miley 1984; *i*, Høgbom 1979; *j*, Bridle, Perley, and Henriksen; *k*, Laing and Bridle 1987; *l*, Biretta, Owen, and Hardee 1983; *m*, Saslaw, Tyson, and Crane 1978; *n*, Heckman *et al.* 1982; *o*, Harris 1972; *p*, R. Perley, private communication 1987.

Col. (6):—Total radio luminosity in ergs s⁻¹. See text for details.

Col. (7):—Core radio power in ergs s⁻¹ Hz⁻¹.

Col. (8):—Angular extent of radio source in arcseconds, taken from our VLA maps or the radio maps indicated in the individual source descriptions. For sources with hotspots at the very ends of the radio source structure, the extent is taken as the distance between the two hotspots. For sources where the radio emission ends in diffuse emission, the extent is measured between the lowest significant contours. For 3C 218 we give in parentheses the very large scale source size detected by Ekers and Simkin 1985 using the Fleurs synthesis telescope. However, we use throughout the paper the smaller source size for 3C 218, determined from our VLA radio maps, since the nature of the relationship between the small-scale structure of 3C 218 and the larger tail, or halo, is uncertain, and almost all of the source flux is contained in the small scale "head" region of the source. For 3C 264 we give in parentheses the very large scale source size detected by Gavazzi, Perola, and Jaffe 1981 using the Westerbork synthesis array.

Col. (9):—Linear extent of radio source in kiloparsecs.

Col. (10):—Radio source position angle, in degrees east of north.

Col. (11):—Bending angle of radio source, defined as 180 minus the position angle difference between the line joining each hotspot with the core.

metrically distributed with respect to the galaxy nucleus. We classify the radio morphology of these sources as "AM," for amorphous.

In our combined sample of 43 radio sources, we have 11 FR1, 26 FR2, 2 FR2_{dstb}, 1 FR2?, 2 AM, and one radio source which is unresolved on the 200 pc scale. We have classified each radio source purely on the basis of its radio morphology. However, it is well known that the radio morphology of extragalactic radio sources correlates with total radio power (Fanaroff and Riley 1974). In Figure 1a, we show a histogram of total radio luminosity, where we have distinguished between the FR2, FR2_{dstb}, FR2?, FR1, and AM sources on the plot. We note that there are almost two orders of magnitude in radio

luminosity between the regions of exclusively FR1 and FR2 radio morphologies, with the "transition zone" extending from $\sim 6 \times 10^{41}$ to 5×10^{43} ergs s^{-1} . As might have been expected from their radio morphologies, the FR2_{dstb} and FR2? sources have luminosities in this transition region. Perhaps unexpectedly, the two AM sources also have radio luminosities in the transition zone.

In Figure 1b, we have plotted a histogram of the projected radio source sizes for the sources in our samples, where we have differentiated between the classes of radio morphology. We see (1) the largest (> 400 kpc) sources have exclusively FR2 morphologies, but that there are also sources with FR2 radio morphologies with very small projected source sizes (~ 20 kpc),

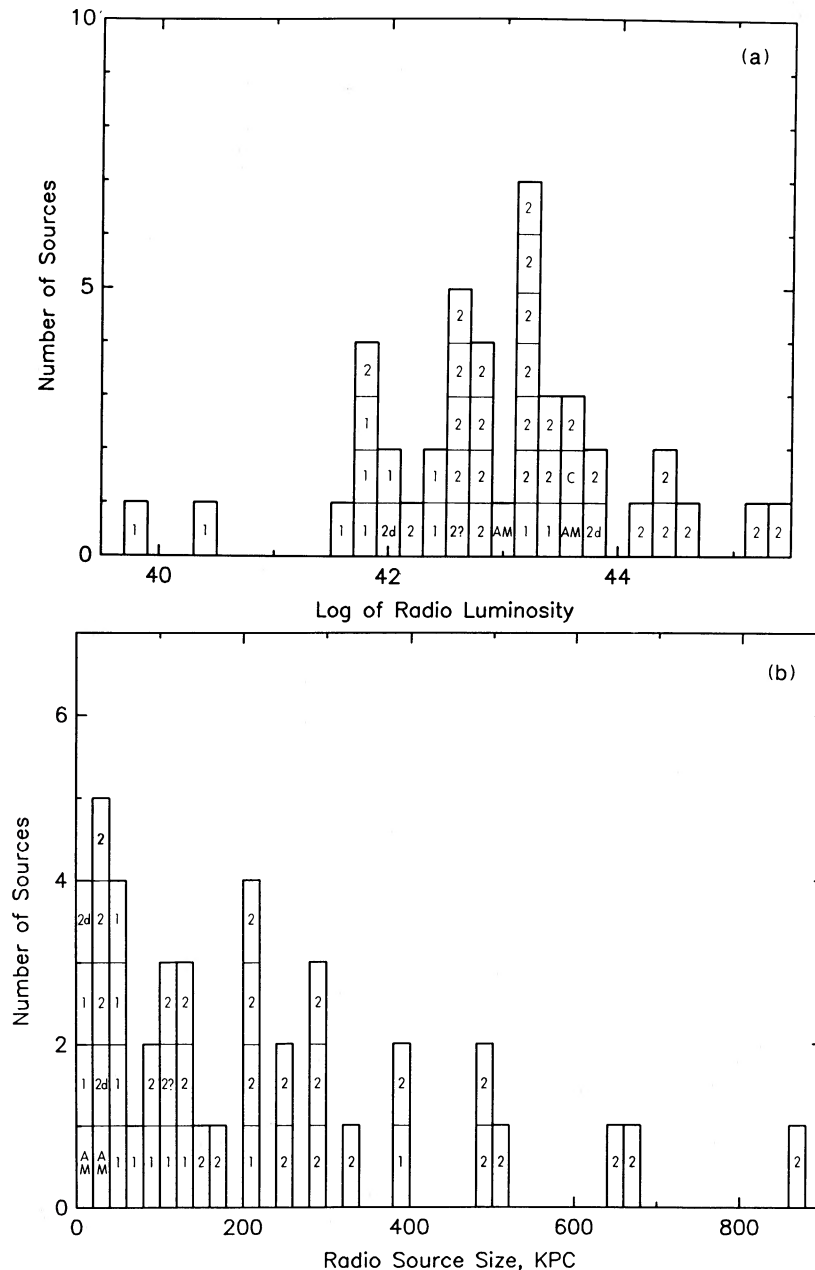


FIG. 1.—Histograms of (a) L_{radio} , the total radio luminosity in ergs s^{-1} , and (b) d_{radio} , the radio source size in kiloparsecs, for the sources from the representative and special samples. The symbol in each box denotes the morphological classification of the radio source, as described in § IIa.

(2) the FR1 sources in our sample range in size from tens of kpc to ~ 400 kpc, and (3) the sources with AM and FR2_{dstb} radio source morphologies are small (< 35 kpc). Gavazzi and Perola (1978) find a correlation between radio source size and radio luminosity for low-redshift ($z < 0.1$) sources. At higher redshifts, Oort *et al.* (1987) find that radio source size increases gradually with radio luminosity, but that source size evolves with redshift, so that the average source size is smaller at higher redshifts. Thus it is not surprising that, for our sample as a whole (a radio flux density limited sample with a range of redshift extending from 0.003 to 0.48 and a median $z \sim 0.06$) we find no significant correlation of radio luminosity with radio source size.

b) Broad-Band Imaging

i) Broad-Band Optical Parameters

We have extracted the R band flux from each calibrated broad band galaxy image. In Table 3, we give the luminosity of each galaxy observed through the R band filter, interior to an absolute surface brightness $\geq 10^{-15}$ ergs s^{-1} cm^{-2} $arcsec^{-2}$, where we have corrected the limiting surface brightness for the $(1+z)^{-4}$ diminution of brightness with redshift, the diminution of R band brightness due to the shift of the observed galaxy spectrum to longer wavelengths, and the shrinking of the effective bandwidth over which the spectrum is integrated (i.e., the K corrections, taken from Whitford 1975), and Galactic reddening (as derived from the E_{B-V} values from Burstein and Heiles 1982 as given in Paper I and the wavelength dependence of the extinction determined by Whitford 1958 as given by Lequeux *et al.* 1979). The corresponding luminosities were corrected for the K corrections and Galactic reddening. In some cases, we have determined the R band luminosity from V band images, using the assumption that the V band luminosity is 1.14 times the R band luminosity (i.e., $V-R = 0.6$). In the cases where a second galaxy is projected on the envelope of the radio galaxy so that we could not separate the contribution from the two galaxies, we give the combined luminosity of the two galaxies.

We have extracted the orientation of the major axis of the galaxy isophotes from each broad-band galaxy image (see Table 3). For 22 of the sources the position angles were determined by fitting an ellipse to the galaxy isophote at 24 mag $arcsec^{-2}$ (taken from Smith 1988). We have also determined each galaxy's orientation by (1) measuring the position angle of the major axis from contour plots of the broad band surface brightness, and (2) fitting two-dimensional Gaussians to the broad-band galaxy images within the region where the surface brightness is 20% of the peak brightness. In most cases, the agreement between these three estimates of the orientation of the galaxy was excellent (within 10°) and in no case was the disagreement greater than 20° . For 17 galaxies where the orientations were not available in Smith (1988), we use the latter two methods to determine the position angle of the galaxy major axis. There remain four galaxies for which an optical position angle could not be determined, either because of inadequate resolution or because of severe distortion of the galaxy's isophotes.

ii) Morphological Peculiarities in the Host Galaxy's Optical Isophotes

Peculiarities in the form of fans, tails, shells, twisted isophotes, dust lanes, or bridges to nearby galaxies (using the terminology of Heckman *et al.* 1986) can be seen in the broad-band images of some of the galaxies in our sample. We have

used the broad-band images of the galaxies, in conjunction with the emission-line images, to determine which galaxies have morphological peculiarities which are *dominated* by continuum (rather than line) emission. We find such peculiarities associated with $\sim 25\%$ of the galaxies from the representative sample (3C 33, 3C 98,⁴ PKS 0745–191, 3C 223, 3C 272.1, PKS 1345+125, 3C 327, 3C 403, and 3C 405) and four out of five of the galaxies from the special sample (3C 285, 3C 305, 3C 171, and 3C 321). These peculiarities in the distribution of the continuum light occur at high levels of surface brightness (typically more than 25 V magnitudes $arcsec^{-2}$, or 3.5×10^{-16} ergs s^{-1} cm^{-2} $arcsec^{-2}$) and are often found outside of the main body of the galaxy. We have not searched for more subtle nonuniformities in the distribution of the continuum light (as described by Lauer 1984; Lauer 1987; Ebeneter, Djorgovski, and Davis 1988), and we have not included galaxies in which the only sign of distortion is a radial change in the ellipticity or orientation of elliptical isophotes.

In an additional 16% of the galaxies from the representative sample (i.e., in 3C 40, 3C 75, 3C 264, 3C 278, 3C 433, and 3C 442), the host galaxy has a second galaxy projected within its stellar isophotes, within 25 kpc of the host galaxy nucleus. Finally, PKS 0745–191, 3C 196.1, 3C 218, 3C 227, PKS 1345+125, 3C 317, and 3C 346 (an additional 18% of the representative sample) are *potential* multiple nuclei galaxies; i.e., an unresolved continuum source can be seen projected within each galaxy's stellar envelope within 15 kpc of the host galaxy nucleus. In 3C 317 the secondary nucleus has been shown to have a radial velocity only 65 $km s^{-1}$ different from the primary nucleus (Hoessel, Kirk, and Schneider 1985), but in all of the other sources, the redshift of the potential secondary nucleus has not been measured.

iii) The Orientation of the Radio Source with Respect to the Host Galaxy Isophotes

In Figure 2, we show histograms of the position angle difference between the radio source position angle and the major axis of the broad-band galaxy image for the sample as a whole, and for various subsets of our sample. For the sample as a whole, we find no preferential alignment of the radio source axis and the isophotes of the host galaxy. Chambers, Miley, and van Breugel (1987) and McCarthy *et al.* (1988) report that in high redshift (median redshift ~ 1) radio galaxies, the radio source axis is aligned along the major axis of the optical light distribution. We find no difference in the distribution of the radio source axis with respect to the galaxy isophotes for galaxies at redshifts less than 0.1 and galaxies at redshifts greater than 0.1.

We do find slight tendencies for the radio source to align with the minor axis of the host galaxy in sources with FR2 radio source structures and in sources in which the radio source is greater than 200 kpc in length (these subsamples necessarily have members in common). Assuming simple binomial statistics with an equal probability of finding a position angle difference greater than or less than 45° , we find that a distribution closer to the mean than observed would occur $\sim 95\%$ of the time by chance for the subset of sources which are greater than 200 kpc in total length. It appears that the linear size of the radio source, rather than the FR2 radio morphology, is the characteristic which is related to the source-minor axis alignment; in four out of the nine radio galaxies

⁴ Though the broad-band image of 3C 98 displayed in Paper I does not show any peculiarities, deeper images show a faint shell (Smith 1988).

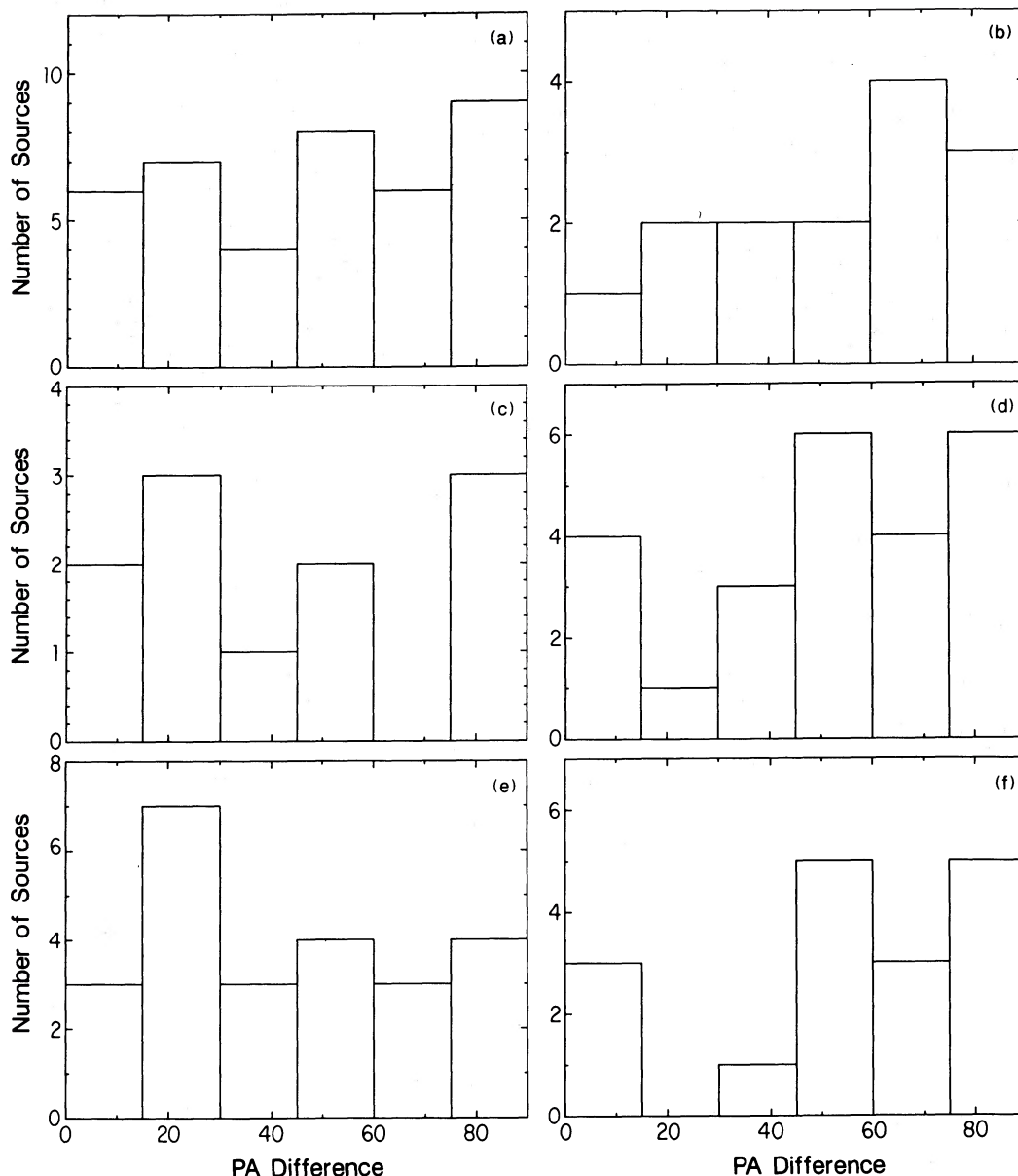


FIG. 2.—Histograms of the position angle difference between the radio axis and the major axis of the host galaxy's isophotes for the following subsets of the representative sample: (a) all extended radio sources, (b) sources associated with galaxies at $z > 0.1$, (c) sources with FR1 morphologies, (d) sources with FR2 morphologies, (e) sources with $d_{\text{radio}} < 200$ kpc, (f) sources with $d_{\text{radio}} > 200$ kpc.

with FR2 radio sources whose linear extent is less than 200 kpc, the radio source is askew to the galaxy minor axis by 45° or more. This result supports Palimaka *et al.* (1979) who found in a sample of 78 radio galaxies (eight in common with our sample⁵) that the trend toward minor-axis alignment of the radio source was strongest in radio sources with linear extents greater than 200 kpc. However, we find *no* tendency for sources less than 200 kpc in total extent to align with the galaxy minor axis. Finally, Kapahi and Saikia (1982) found that the radio source axis in radio sources with strong cores (relative to their

total source flux), aligns with the minor axis of the host galaxy. Less than a handful of the sources from our sample satisfy the criterion for core dominance as defined by Kapahi and Saikia, and we are therefore unable to look for this trend in our data.

c) Optical Emission-Line Imaging

i) Parameterization of the Optical Emission-Line Images

The results of the emission-line survey are presented in Tables 2 and 3. We give the equivalent width and flux of the line emission with a $3''$ by $3''$ square centered on the galaxy nucleus (not corrected for Galactic reddening). We also give (1) the equivalent width and the total flux in emission lines (not corrected for Galactic reddening), interior to an absolute

⁵ While our measured optical and radio position angles are in good agreement with those of Palimaka *et al.* (1979) for six sources, we disagree with their determination of the position angle for the minor axes of the host galaxies of 3C 219 and 3C 223.

TABLE 2
OPTICAL RESULTS

Source	Lines Imaged	Correction to Line Flux	Line Flux inner 3" ergs s ⁻¹ cm ⁻²	EQW inner 3" Å	Line Flux Total ergs s ⁻² cm ⁻²	EQW Total Å
3C 29 *	Hα + [NII] ^b	1.09	4.0 × 10 ⁻¹⁵	7	5.4 × 10 ⁻¹⁵	6
3C 33 *	Hα + [NII] ^c	1.09	3.1 × 10 ⁻¹⁴	76	6.0 × 10 ⁻¹⁴	54
3C 40 *	Hα + [NII] ^b	1.29	6.5 × 10 ⁻¹⁵	3	2.9 × 10 ⁻¹⁴	3
B2 0149 + 358	Hα + [NII] ^c	1.09	1.7 × 10 ⁻¹⁴	24	7.0 × 10 ⁻¹⁴	10
3C 63 *	Hα + [NII] ^c	1.14	9.8 × 10 ⁻¹⁵	110	1.9 × 10 ⁻¹⁴	112
3C 75N *	Hα + [NII]	1.27	unresolved	...	1.7 × 10 ⁻¹⁵	...
3C 75S *	Hα + [NII]	1.27	unresolved	...	1.7 × 10 ⁻¹⁵	...
3C 78 *	Hα + [NII] ^c	1.34	1.3 × 10 ⁻¹⁴	8	2.8 × 10 ⁻¹⁴	6
3C 88 *	Hα + [NII] ^c	1.28	1.8 × 10 ⁻¹⁴	46	2.8 × 10 ⁻¹⁴	23
3C 89 *	Hα + [NII] ^b	1.003	unresolved	...	5.0 × 10 ⁻¹⁵	3
PKS 0349 - 278 *	[OIII] ^{a,c}	...	7.8 × 10 ⁻¹⁵	...	8.4 × 10 ⁻¹⁴	...
3C 98 *	Hα + [NII] ^c	1.09	2.0 × 10 ⁻¹⁴	23	3.5 × 10 ⁻¹⁴	17
3C 105 *	Hα + [NII]	1.02	unresolved	...	4.0 × 10 ⁻¹⁵	45
3C 109 *	[OIII]	1.01	2.4 × 10 ⁻¹⁴	136	4.4 × 10 ⁻¹⁴	185
PKS 0634 - 206 *	Hα + [NII] ^c	1.38	1.6 × 10 ⁻¹⁴	79	7.7 × 10 ⁻¹⁴	52
3C 171	[OIII] ^{a,c}	1.09	2.6 × 10 ⁻¹⁴	1365	4.6 × 10 ⁻¹⁴	1459
PKS 0745 - 191 *	Hα + [NII] ^c	1.01	3.3 × 10 ⁻¹⁴	288	9.8 × 10 ⁻¹⁴	146
3C 192 *	Hα + [NII] ^c	1.09	2.4 × 10 ⁻¹⁴	41	3.1 × 10 ⁻¹⁴	33
3C 196.1 *	Hα + [NII] ^c	1.03	2.8 × 10 ⁻¹⁵	45	5.7 × 10 ⁻¹⁵	53
3C 218 *	Hα + [NII] ^{c,d}	1.31	1.6 × 10 ⁻¹⁴	25	2.3 × 10 ⁻¹⁴	10
3C 219 *	Hα + [NII]	1.36	unresolved	...	1.8 × 10 ⁻¹⁴	125
3C 223 *	Hα + [NII] ^b	1.35	2.0 × 10 ⁻¹⁴	153	2.4 × 10 ⁻¹⁴	101
3C 227 *	Hα + [NII] ^c	1.05	6.6 × 10 ⁻¹⁴	70	1.2 × 10 ⁻¹³	95
3C 264 *	Hα + [NII] ^{c,d}	1.27	8.0 × 10 ⁻¹⁵	6	1.3 × 10 ⁻¹⁴	5
3C 272.1 *	Hα + [NII] ^{a,c}	...	3.6 × 10 ⁻¹⁴	15	1.2 × 10 ⁻¹³	6
3C 274 *	Hα + [NII] ^c	1.09	1.3 × 10 ⁻¹³	30	8.0 × 10 ⁻¹³	4
3C 275 *	[OIII]	1.004	>7.9 × 10 ⁻¹⁵	782	>1.2 × 10 ⁻¹⁴	602
3C 278 *	Hα + [NII] ^b	1.10	1.5 × 10 ⁻¹⁴	3	2.6 × 10 ⁻¹⁴	4
3C 285	Hα + [NII] ^c	1.08	6.3 × 10 ⁻¹⁵	41	1.9 × 10 ⁻¹⁴	41
PKS 1345 + 125 *	Hα + [NII] ^{a,c}	...	8.0 × 10 ⁻¹⁵	59	4.4 × 10 ⁻¹⁴	101
3C 295 *	[OIII] ^b	1.01	1.8 × 10 ⁻¹⁵	45	2.2 × 10 ⁻¹⁵	41
3C 305	Hα + [NII] ^{a,c}	...	6.5 × 10 ⁻¹⁴	42	2.2 × 10 ⁻¹³	45
3C 313 *	[OIII]	1.01	2.2 × 10 ⁻¹⁵	40	3.4 × 10 ⁻¹⁵	52
3C 317 *	Hα + [NII] ^{a,c}	...	1.4 × 10 ⁻¹⁴	60	2.6 × 10 ⁻¹⁴	31
3C 321	Hα + [NII] ^{a,c}	...	6.8 × 10 ⁻¹⁴	...	1.6 × 10 ⁻¹³	51
3C 327 *	Hα + [NII] ^{a,d}	...	4.1 × 10 ⁻¹⁴	88	6.0 × 10 ⁻¹⁴	48
3C 327.1 *	[OIII]	1.01	unresolved	...	3.6 × 10 ⁻¹⁵	240
3C 346 *	Hα + [NII] ^b	1.002	>1.7 × 10 ⁻¹⁵	41	>1.9 × 10 ⁻¹⁵	11
3C 353 *	Hα + [NII] ^c	1.28	1.4 × 10 ⁻¹⁵	52	1.7 × 10 ⁻¹⁴	36
3C 390.3 *	[OIII] ^{a,d}	...	unresolved	...	2.7 × 10 ⁻¹³	165
3C 403 *	Hα + [NII] ^c	1.08	>7.9 × 10 ⁻¹⁵	38	>1.2 × 10 ⁻¹⁴	25
3C 405 *	[OIII] ^{a,c,d}	1.6 × 10 ⁻¹³	321
3C 433 *	Hα + [NII] ^c	1.01	1.9 × 10 ⁻¹⁴	113	4.4 × 10 ⁻¹⁴	64
3C 442 *	Hα + [NII] ^c	1.09	8.6 × 10 ⁻¹⁵	10	2.2 × 10 ⁻¹⁴	7

Col. (1).—Source name. An asterisk designates membership in the representative sample.

Col. (2).—Lines imaged. Hα + [N II] signifies Hα λ6563, [N II] λ6548, and λ6584; [O III] signifies [O III] λ5007. An "a" superscript indicates that the observations were calibrated using spectrophotometry from the literature. Specifically, the following sources were calibrated using the results presented in the following references: PKS 0349 - 278, Danziger *et al.* 1984; 3C 171, Yee and Oke 1978; 3C 272.1, Hansen, Noorgard-Nielsen, and Jorgensen 1985; PKS 1345 + 125, Grandi 1977 and Gilmore and Shaw 1986; 3C 305, Heckman *et al.* 1982; 3C 317, Cohen and Osterbrock 1981; 3C 321, van Breugel 1987, private communication; 3C 327, Costero and Osterbrock 1977; 3C 390.3, Yee and Oke 1978; 3C 405, Osterbrock and Miller 1975. A "b" superscript indicates that the results are uncertain and require spectroscopic confirmation. A "c" superscript indicates that we have spectroscopic confirmation that the galaxy has resolved emission-line gas. A "d" superscript indicates that one or all of the emission lines imaged fell outside of the main response of the narrow-band filter. Specifically, the following lines in the following sources fell on the edge of the filter response; [N II] λ6548 in 3C 218, 3C 264, and 3C 327, and [O III] λ5007 in 3C 171, 3C 390.3, and 3C 405. 3C 275, 3C 346, and 3C 403 were observed under nonphotometric conditions. We therefore can list only lower limits to the flux in emission lines from these sources.

Col. (3).—Factor that would need to be applied to the emission line fluxes to correct for oversubtraction due to the use of a broad-band filter to subtract the continuum from the narrow-band images, assuming line ratios of an average nuclear narrow emission-line radio galaxy. See text for more details.

Col. (4).—The observed flux in emission lines from a 3" by 3" (projected) square, centered on the galaxy's nucleus.

Col. (5).—The average value of the equivalent width of the emission lines in the inner 3" (as described above). We have determined the equivalent width as

$$\frac{F_{\text{lines}}}{cF_{\text{bb}}} \Delta_{\text{bb}},$$

where F_{lines} is the flux in emission lines, F_{bb} is the flux in the broad-band image, and Δ_{bb} is the width of the broad-band filter in angstroms. The factor c , defined as one minus the ratio of flux in emission lines in the broad-band image to the total flux in the broad-band image, corrects for the contamination of the broad-band image by emission lines. To calculate c we assume the emission-line gas has a spectrum typical of the nuclei of narrow-line radio galaxies. For 3C 227 we give estimates of the equivalent widths in narrow lines only.

Col. (6).—The total flux in emission lines (not corrected for galactic reddening) interior to a dereddened absolute surface brightness of $10^{-16}(1+z)^{-4}$ ergs s⁻¹ cm⁻² arcsec⁻². For 3C 75 we list the emission-line fluxes measured by W. Keel (1987, private communication), since difficulties in the subtraction process made estimation of the line flux difficult.

Col. (7).—The average equivalent width (as defined above) of the emission lines interior to a dereddened absolute surface brightness of $10^{-16}(1+z)^{-4}$ ergs s⁻¹ cm⁻² arcsec⁻².

TABLE 3
OPTICAL RESULTS 2

Source	L_{lines}	$f_{r \leq 2.5}$	$f_{r \geq 5}$	Size "	Size kpc	$L_{\text{lines}}/L_{\text{radio}}$ $\times 100$	$L_{R\text{band}}$	BB PA
3C 29 *	2.3×10^{40}	0.90	0.07	9.0	7.3	0.6	5.6×10^{43}	113
3C 33 *	4.6×10^{41}	0.71	0.01	10.5	11.1	3.1	2.6×10^{43}	147
3C 40 *	2.0×10^{40}	0.98	0.00	10.5	3.5	5.1	$5.4 \times 10^{43} \text{ }^a$	110
B2 0149 + 358	3.8×10^{40}	0.85	0.14	26.0	8.0	405.2	2.7×10^{43}	46
3C 63 *	1.3×10^{42}	...	0.43	16.8	45.0	3.4	3.0×10^{43}	100
3C 75 *	4.3×10^{39}	1.00	0.00	≤ 1.7	≤ 0.8	0.5	$2.8 \times 10^{43} \text{ }^b$	97n, 155s
3C 78 *	5.4×10^{40}	0.96	0.00	8.9	4.8	1.9	$4.6 \times 10^{43} \text{ }^a$	152
3C 88 *	6.1×10^{40}	0.98	0.001	5.5	3.1	3.7	$1.7 \times 10^{43} \text{ }^a$	151
3C 89 *	2.3×10^{41}	1.00	0.00	≤ 1.4	≤ 3.1	1.4	6.1×10^{43}	36
PKS 0349 - 278 *	7.5×10^{41}	0.11	0.73	35.0	40.8	13.8
3C 98 *	8.6×10^{40}	0.92	0.06	26.5	15.1	2.7	1.2×10^{43}	55
3C 105 *	8.7×10^{40}	1.00	0.00	≤ 2.8	≤ 4.2	0.6	$5.5 \times 10^{42} \text{ }^a$	47
3C 109 *	1.3×10^{43}	...	0.70	8.8	35.3	9.8	...	145
PKS 0634 - 206 *	1.3×10^{42}	0.37	0.34	39.6	39.7	17.1	$2.6 \times 10^{43} \text{ }^a$	0
3C 171	7.8×10^{42}	...	0.48	13.0	43.9	14.8	2.7×10^{43}	165
PKS 0745 - 191 *	2.8×10^{42}	...	0.38	13.5	22.7	34.2	...	85
3C 192 *	2.4×10^{41}	0.87	0.08	17.4	18.5	6.0	2.0×10^{43}	135
3C 196.1 *	5.7×10^{41}	...	0.48	4.5	13.2	1.3	$7.6 \times 10^{43} \text{ }^a$	57
3C 218 *	1.5×10^{41}	0.80	0.05	13.5	13.2	0.49	$2.8 \times 10^{43} \text{ }^a$	145
3C 219 *	1.2×10^{42}	1.00	0.00	≤ 1.5	≤ 4.0	1.6	$4.7 \times 10^{43} \text{ }^a$	124
3C 223 *	9.9×10^{41}	...	0.08	4.6	10.1	5.3	$1.6 \times 10^{43} \text{ }^a$	50
3C 227 *	7.0×10^{41}	0.27	0.36	63.0	96	4.3	2.1×10^{43}	177
3C 264 *	1.1×10^{40}	1.00	0.00	6.3	2.4	1.9	$8.1 \times 10^{43} \text{ }^a, \text{ }^b$	152
3C 272.1 *	2.2×10^{39}	1.00	0.00	24.5	1.5	10.1	...	127
3C 274 *	1.9×10^{40}	0.95	...	198.0	13.9	3.0
3C 275 *	$\geq 8.5 \times 10^{42}$	4.4	23.5	≥ 3.0	...	147
3C 278 *	1.1×10^{40}	1.00	0.00	6.9	1.9	1.8	$6.5 \times 10^{43} \text{ }^b$	165
3C 285	2.5×10^{41}	0.24	0.46	13.2	18.2	4.7	2.4×10^{43}	133
PKS 1345 + 125 *	1.4×10^{42}	...	0.34	8.8	17.5	3.1
3C 295 *	1.4×10^{42}	3.1	16.1	0.1	1.1×10^{44}	...
3C 305	7.8×10^{41}	0.66	0.06	18.4	13.8	62.3	...	74
3C 313 *	2.1×10^{42}	...	0.68	4.0	20.6	0.8	1.8×10^{44}	180
3C 317 *	6.4×10^{40}	0.85	0.06	23.0	14.8	2.9	...	33
3C 321	3.4×10^{42}	0.30	0.43	32.0	52.0	24.6	...	18
3C 327 *	1.6×10^{42}	...	0.00	3.9	6.8	7.5	...	135
3C 327.1 *	2.6×10^{42}	≤ 1.5	≤ 7.8	0.8	4.1×10^{43}	152
3C 346 *	$\geq 1.2 \times 10^{41}$...	0.00	3.0	7.5	≥ 0.4	...	126
3C 353 *	4.2×10^{40}	1.00	0.00	7.4	4.2	0.3	$4.7 \times 10^{42} \text{ }^a$	82
3C 390.3 *	2.0×10^{42}	1.00	0.00	≤ 1.5	≤ 1.5	25.6	$2.4 \times 10^{43} \text{ }^a$	97
3C 403 *	$\geq 1.6 \times 10^{41}$	0.81	0.001	13.0	13.7	≥ 3.5	...	22
3C 405 *	2.9×10^{42}	0.78	0.00	8.5	8.6	0.2	...	152
3C 433 *	9.9×10^{41}	0.38	0.32	13	22.0	2.5	...	147
3C 442 *	3.4×10^{40}	0.98	0.00	10.0	4.9	5.2	$6.7 \times 10^{43} \text{ }^b$	131

Col. (1):—Source name. An asterisk denotes membership in the representative sample.

Col. (2):—Emission-line luminosity of the entire nebula. The luminosity in the emission line(s) specified in col. (2) of Table 5, corrected for Galactic reddening, and interior to a dereddened absolute surface brightness of $10^{-16}(1+z)^{-4}$ ergs $\text{s}^{-1} \text{cm}^{-2} \text{arcsec}^{-2}$. For 3C 227 we give the $H\alpha$ + [N II] luminosity in narrow lines only.

Col. (3):—The fraction of the narrow emission-line luminosity which is emitted from within 2.5 (projected) kpc of the galaxy nucleus.

Col. (4):—The fraction of the narrow emission-line luminosity which is emitted from beyond 5.0 (projected) kpc of the galaxy nucleus.

Col. (5):—Angular size of the emission-line nebula in arcseconds. The angular size of the emission-line nebula interior to a dereddened absolute surface brightness of $10^{-16}(1+z)^{-4}$ ergs $\text{s}^{-1} \text{cm}^{-2}$.

Col. (6):—Linear size of emission-line nebula in kiloparsecs.

Col. (7):—The ratio of the luminosity in the measured narrow emission line(s) to the total radio luminosity, times 100.

Col. (8):—R band optical luminosity. The absolute R band luminosity, interior to an absolute surface brightness of 10^{-15} ergs $\text{s}^{-1} \text{cm}^{-2} \text{arcsec}^{-2}$, where we have corrected the limiting surface brightness for the $(1+z)^{-4}$ diminution of brightness with redshift, Galactic reddening, and the K corrections for the shrinking of the effective bandwidth over which the spectrum is integrated and the shift of the observed galaxy spectrum to longer wavelengths. We have corrected the corresponding luminosities for the K corrections and Galactic reddening. A superscript *a* indicates R band luminosity was determined from a V band image, using an assuming the absolute V magnitude of the galaxy is given by the absolute R magnitude plus 0.6. A superscript *b* indicates that the R band luminosity given is of the host radio galaxy plus a second galaxy which is superposed on the envelope of the radio galaxy.

Col. (9):—The position angle of the major axis of the host galaxy (see text for more details).

surface brightness of $10^{-16} \times (1+z)^{-4}$ ergs s^{-1} cm^{-2} arcsec $^{-2}$ (where we have corrected the absolute surface brightness for Galactic reddening), (2) the corresponding line luminosity, corrected for Galactic reddening, (3) the fraction of the line luminosity which comes from within 2.5 projected kpc, and (4) the fraction of line luminosity which originates from beyond 5 projected kpc of the galaxy nucleus.

Finally we have measured the diameters (taken as the maximum extent) of the emission-line nebulae (d_{neb}), interior to a dereddened, absolute surface brightness of $10^{-16}(1+z)^{-4}$ ergs s^{-1} cm^{-2} arcsec $^{-2}$. For sources in which the apparent angular size of the emission-line nebula is only slightly larger than the PSF, we deconvolved the diameter of the emission-line nebula from the PSF by assuming that both possess Gaussian shapes. The linear diameter of an emission-line nebula, as we have defined it, would be a distance independent

property if the nebulae were surfaces whose brightness fell off with radius in a smooth and predictable manner. However, many of the nebulae are filamentary in structure. Thus, at higher redshifts and in images of low angular resolution, emission-line features may be lost against the background sky noise due to the decrease in linear resolution.

ii) Optical Emission-Line Properties

Considering only the sources from the representative sample, we can make the following general statements. We detect emission-line gas in *all* of the sources we observed, although in some sources (as noted in Table 2) the results still need to be confirmed spectroscopically. In Figure 3a, we plot a histogram of the integrated line luminosities. The line luminosities in $H\alpha + [N II]$ or $[O III]$ (as specified in col. [2] of Table 2) range from 2.2×10^{39} to 1.3×10^{43} ergs s^{-1} , and the median line luminosity is $\sim 3 \times 10^{41}$ ergs s^{-1} .

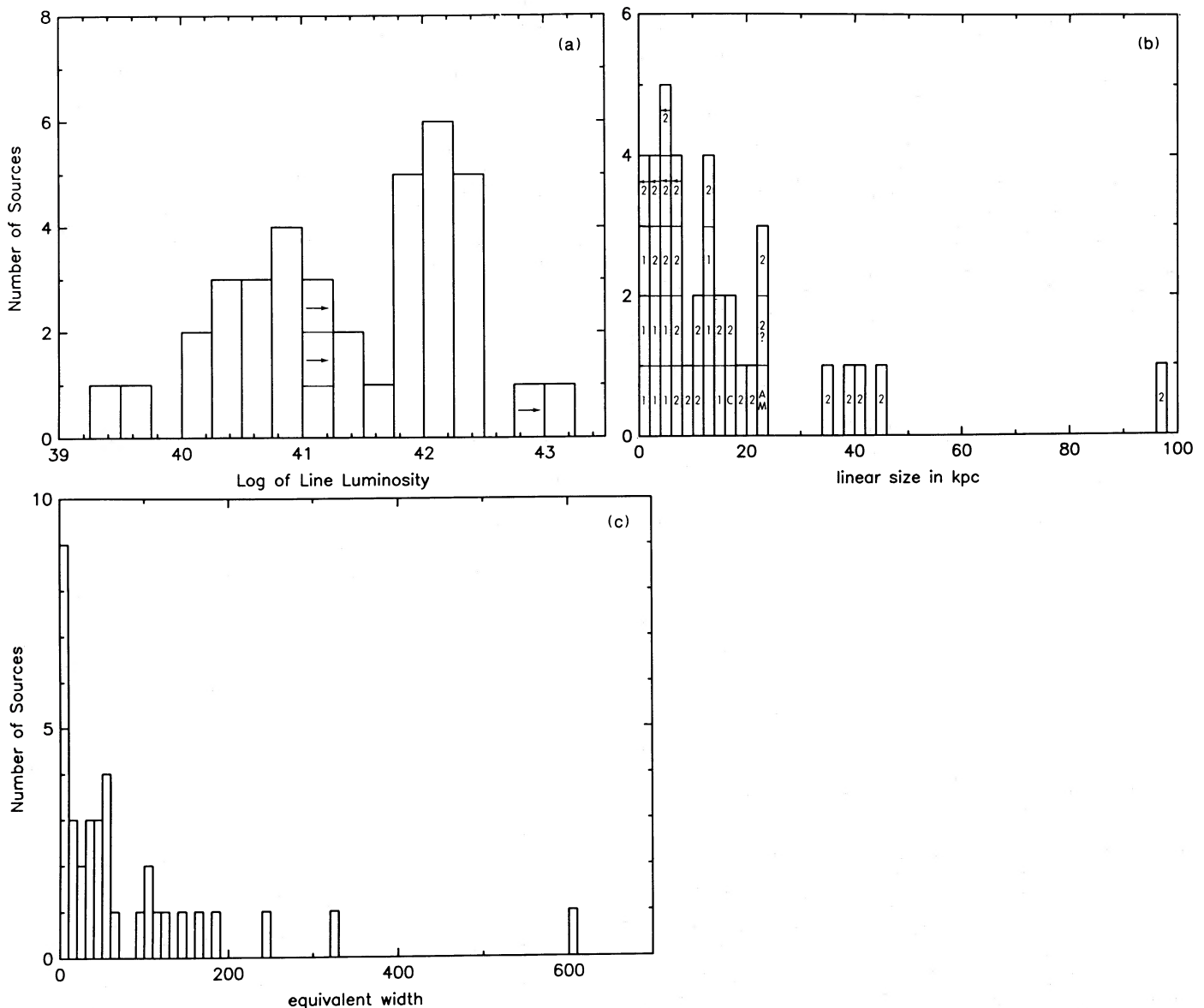


FIG. 3.—(a) Histogram of L_{line} , the narrow-line luminosity in $H\alpha + [N II]$ or $[O III]$ in ergs s^{-1} , for the sources from the representative sample. (b) Histogram of d_{neb} , the linear size of the emission-line nebula in kiloparsecs, for the sources from the representative sample. (c) Equivalent width of the emission-line nebulae ($H\alpha + [N II]$ or $[O III]$) for the sources from the representative sample.

In 32 out of the 38 sources in the representative sample, or $\sim 85\%$ of the sources, we have resolved the emission-line nebula, although, for six of the 32 sources we do not yet have spectroscopic confirmation that the emission line regions are extended (see col. [2], Table 2). In Figure 3b, we show a histogram of the isophotal diameters of the emission-line nebulae. The nebulae range in size from less than 1 to 96 kpc, with a median extent of ~ 10 kpc. If we divide the sources on the basis of their radio morphologies, we find that the median extent for the emission-line nebulae in the FR1 sources is only ~ 3.5 kpc, while for the FR2, FR2_{dstb}, FR2?, and AM sources the median extent is ~ 14 kpc. All five of the nebulae which are greater than 30 kpc in total extent are associated with sources having FR2 radio morphologies. Not surprisingly, we also find that the higher power radio sources ($L_{\text{radio}} > 10^{42.7}$ ergs s^{-1}) also show a larger median extent of their associated emission-line nebulae (median $d_{\text{neb}} \sim 14$ kpc) than do their lower power counterparts (median $d_{\text{neb}} \sim 5$ kpc). There are not enough intermediate radio power sources with FR1 morphologies in our sample to determine whether the increase in the median emission-line nebula size is linked independently to the radio power or the radio morphology.

The emission-line nebulae in the sources in the representative sample span a range in extent and morphology. In some we observe only small, centrally condensed, kpc scale "oval" regions of line emission, while in others we detect much more extensive filaments of line-emitting gas tens of kiloparsecs from the host galaxy nucleus. If we consider only the sources in the representative sample which have small emission-line nebulae (i.e., sources with $d_{\text{neb}} \lesssim 10$ kpc), then we find that these small nebulae are typically centered on and roughly symmetric about their host galaxy nuclei. Often these small regions of emission-line gas have roughly "elliptical" or "oval" shapes. In contrast, the sources from the representative sample with larger emission-line nebulae (i.e., $d_{\text{neb}} \gtrsim 10$ kpc) tend to be filamentary in appearance, and the very extended line-emitting gas in these sources is typically asymmetrically distributed with respect to the host galaxy nucleus. The smooth appearance of the smaller emission-line nebulae may be, in part, an effect of insufficient angular and linear resolution in the observations.

In Figure 3c, we show a histogram of the equivalent widths of the emission-line nebulae. The measured equivalent widths over the nebulae range from 3 Å to 602 Å, with a median value of ~ 35 Å. By comparing the equivalent width within 3" of the galaxy nucleus to the equivalent width determined over the entire nebula for the sources from the representative sample, we find that in 25 cases the equivalent width either rises or remains constant in moving toward the center of the galaxy, and in only five sources is the equivalent width higher off the galaxy nucleus than on it. Thus, typically, the brightness of the emission-line gas drops more rapidly with distance from the host galaxy nucleus than does the starlight.

As an indication of the distribution of the emission-line flux with distance from the galaxy nucleus, we have also determined and plot as a histogram in Figure 4, the ratio of the emission-line flux within a projected radius of 2.5 kpc of the galaxy nucleus to the total emission-line flux, for each galaxy in the representative sample. The values of this ratio range from 0.1 to 1.0, with a median value of ~ 0.94 . Thus, in most cases, the majority of the emission-line luminosity comes from the gas within 2.5 kpc of the galaxy nucleus. If, however, we consider only the sources having emission-line nebulae greater

than 10 kpc in total extent, we find a median value for the fraction of emission-line flux which originates within 2.5 kpc of no more than 0.70. Thus, we find that in sources with very extended emission-line nebula, typically, at most two-thirds of the total narrow emission-line luminosity comes from within 2.5 kpc of the nucleus. Further, in 10 of these sources, over 30% of the line flux comes from beyond 5 projected kpc of the galaxy nucleus (see Fig. 4b).

iii) Comparison with Normal Early-Type Galaxies

We can compare the emission-line luminosities of these radio galaxies with the line luminosities of normal elliptical and lenticular galaxies. Phillips *et al.* (1986) conducted a spectroscopic survey of an optical magnitude limited sample of early-type galaxies. We interpolate their bivariate luminosity function of absolute blue magnitude and [N II] (6548 Å) luminosity, and conclude that for normal early-type galaxies having absolute blue magnitudes between -20.75 and -21.75 (for $H_0 = 75$), the median [N II] luminosity is $\sim 5 \times 10^{39}$ ergs s^{-1} , while for early-type galaxies having absolute blue magnitudes between -19.75 and -20.75 , the median [N II] luminosity is $\sim 1.5 \times 10^{39}$ ergs s^{-1} . Binning our radio galaxies in absolute blue magnitude in the same way,⁶ we find median [N II] luminosities of 5×10^{40} and 2.5×10^{40} ergs s^{-1} , respectively, including only the line flux within a projected distance of 2.5 kpc from the galaxy nucleus, and assuming line ratios of [N II] $\lambda 6584$ to H α to [N II] $\lambda 6548$ to [O III] $\lambda 5007$ of 0.8:1:0.1:3.8. Thus, the line luminosities in powerful radio galaxies appear to be ~ 10 times greater than the line luminosities in normal early type galaxies of similar absolute magnitude.

Typical equivalent widths of [N II] $\lambda 6584$ in normal elliptical and lenticular galaxies appear to be $\lesssim 2$ Å (Phillips *et al.* 1986). For comparison, the median H α + [N II] equivalent width (within the inner 3") in our sample is ~ 50 Å, giving an approximate equivalent width of ~ 20 Å in [N II] $\lambda 6584$, or again, ~ 10 times the value found in normal early-type galaxies.

Phillips *et al.* (1986) also obtained information on the spatial extent of the emission-line nebulae in their sample, along one slit position. They conclude that the diameter of the emission-line nebulae in normal lenticular and elliptical galaxies is typically $\lesssim 1$ kpc. Demoulin-Ulrich, Butcher, and Boksenberg (1984) obtained images of 11 nearby ellipticals in emission lines, some of which are normal (i.e., inactive), and some of which are active. They report extended regions of ionized gas, with diameters between 1 and 3 kpc for six of the 12 galaxies. In contrast, we find that the median extent of the emission-line nebulae in powerful radio galaxies is ~ 10 kpc, or ~ 10 times the extent of the nebulae in normal early-type galaxies. We note that Phillips *et al.* (1986) were able to detect emission-line gas at much smaller equivalent widths than we; thus the smaller sizes of the emission-line nebulae they observed in normal early-type galaxies do not reflect a lower sensitivity to emission.

d) Correlations

i) Summary of Results

In Table 4, we list the significance of the correlations between the total radio luminosity, the radio luminosity of the core, the optical narrow emission-line luminosity, the broad-

⁶ We have estimated the blue magnitudes from V magnitudes taken from the literature, under the assumption that $M_V + 0.9 = M_B$.

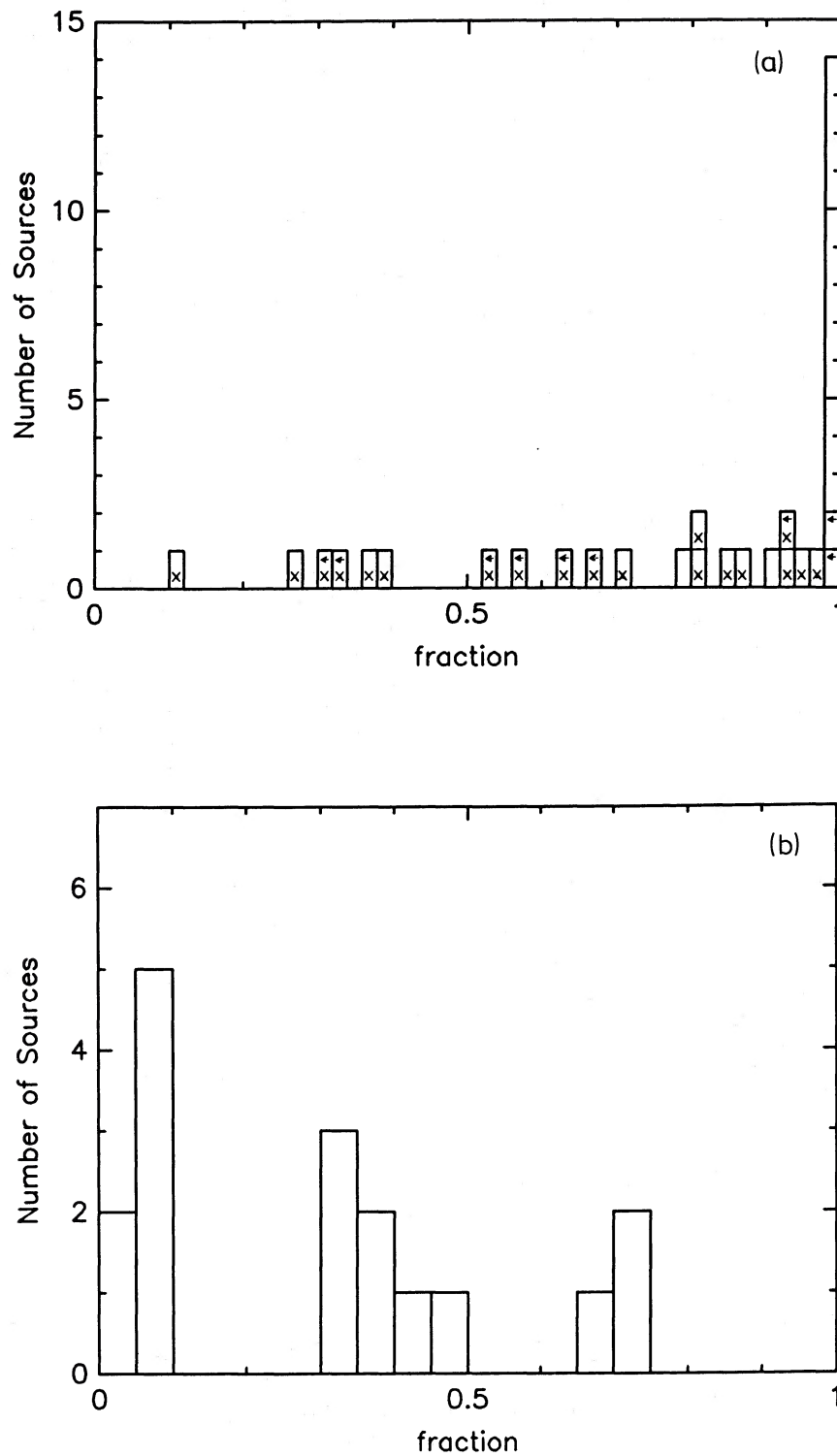


FIG. 4.—(a) Histogram showing the fraction of the narrow emission-line luminosity which originates within 2.5 projected kpc of the galaxy nucleus, for the sources for the representative sample. Nebulae with $d_{\text{neb}} > 10$ kpc are marked, and limits are indicated as arrows, where the midpoint of the arrow is located at the location of the limit. (b) Histogram showing the fraction of the narrow emission-line luminosity which originates beyond 5 projected kpc of the galaxy nucleus for those sources from the representative sample with $d_{\text{neb}} > 10$ kpc.

TABLE 4
CORRELATIONS

	L_{radio}	L_{lines}	$P_{\text{core radio}}$	$L_{R \text{ band}}$	Redshift
L_{radio}	...	$< 1 \times 10^{-7}$ (38)	2×10^{-5} (36)	7×10^{-3} (20)	$< 1 \times 10^{-7}$ (38)
L_{lines}	7×10^{-4} (36)	6×10^{-2} (20)	$< 1 \times 10^{-7}$ (38)
$P_{\text{core radio}}$	2×10^{-2} (20)	1×10^{-4} (36)
$L_{R \text{ band}}$	2×10^{-2} (20)
Redshift

NOTES.—Numbers given are the probability that the two parameters are uncorrelated as determined by a two-sided Kendall rank test, taking upper and lower limits into account. In parentheses we give the number of sources used to compute the correlation. The parameters explored are, in order, the logarithm of the radio luminosity, the logarithm of the emission-line luminosity, the logarithm of the core radio power, the logarithm of the host galaxy R band luminosity, and the redshift.

band optical luminosity of the host galaxy, and the redshift for the sources from the representative sample. The correlation coefficient listed is the probability that the two parameters are uncorrelated, as determined by a two-sided, generalized Kendall rank test (Isobe, Feigelson, and Nelson 1986, and references therein), taking upper and lower limits into account.⁷

We confirm the previously observed correlation of radio luminosity with core radio power (Feretti *et al.* 1984 and find the following previously suspected correlations (Hine and Longair 1979; Wilkinson, Hine, and Sargent 1980):

1. The radio luminosity correlates with the optical emission-line luminosity;
2. The core radio power correlates with the optical emission-line luminosity.

The implications of the correlations of emission-line luminosity with radio core and total power will be discussed in detail in Baum and Heckman 1988 (hereafter Paper III).

ii) *Correlations with Redshift*

As expected for a radio flux density selected sample, we find a strong correlation of redshift and radio luminosity. We also find strong correlations of the redshift with the emission-line luminosity and the core radio power. Our sample has not been explicitly selected on the basis of an optical magnitude limit, or on the basis of the radio core or optical emission-line fluxes of the sources. Further, we have detected all of the radio galaxies in optical emission lines, and only two of the sources have undetected radio cores. Thus, correlations between radio luminosity and the core radio power and emission-line luminosity should not merely be artifacts of the data acquisition. There is no evidence or reason to expect the radio core power and the emission-line luminosity to correlate with redshift over the redshift range covered in our sample ($z_{\text{max}} = 0.48$, $z_{\text{median}} = 0.06$). Thus, it is likely that the strong correlations of redshift with emission-line luminosity and radio core power are secondary correlations induced by the independent correlations of total radio luminosity with line luminosity and core radio power. In order to *unambiguously* determine whether the primary correlations of the emission-line luminosity and the radio core power are with the total radio luminosity rather than the redshift, we would need to observe low-luminosity radio galaxies at high redshifts.

iii) *Correlation of Radio Core and Total Power*

In Figure 5, we plot the total radio luminosity versus the core radio power. As noted above, we find a strong correlation

⁷ The software used for the statistical analysis was kindly provided by T. Isobe and E. Feigelson.

of the core radio power and the total radio luminosity (or total radio power). In order to compare our results directly with those of Feretti *et al.* (1984), we have fit a straight line of the form $\log_{10} P_{\text{core}} = m \log_{10} P_{408} + b$, where P_{408} is the total radio power at 408 MHz in W Hz^{-1} and P_{core} is the core radio power in W Hz^{-1} (using 34 detections and assuming the two upper limits to the core power are detections). We find $m = 0.66 \pm 0.1$ and $b = 6 \pm 3$, in agreement within the errors with the results of Feretti *et al.* (1984) who studied a sample of 96 sources, 12 of which were common to our sample. Thus, the fraction of the total radio power which comes from the core decreases with increasing total radio power. Like Feretti *et al.* we find no evidence for a change in the slope of the relationship as a function of total radio power.

We note that in a radio flux density selected sample such as ours in which we have observed all of the sources at roughly the same angular resolution, we have necessarily observed the higher radio luminosity sources at lower linear resolution. The effect this plays in the observed correlation should be reduced in our sample since we have measured the core fluxes at a high frequency (typically 6 cm) and at fairly high angular resolution (typically, $\sim 1''.5$). In almost all cases, we detect no other radio emission near the core (e.g., from jets), which could potentially be blended with the core emission.

iv) *Correlations with the Optical Continuum Luminosity*

We find no strong correlations of the optical continuum luminosity (i.e., the galaxy R magnitude) with the total radio luminosity, the core radio power, the optical emission-line luminosity, or the redshift. The correlation coefficients listed in Table 4 do not include any of the dumbbell galaxies from our sample, since the estimates of the optical luminosities of the host radio galaxy are very uncertain in these systems. We have consistent optical R band luminosities for only 20 sources from our sample, so our ability to detect weak trends is limited.

We do find weak trends for the optical R band luminosity to increase with both total radio luminosity and core radio power; however, these trends are likely to be influenced by selection effects. Only sources with known identifications and redshifts are included in our sample, implying that at high redshift, and hence high radio luminosity and high radio core power, we have indirectly selected for relatively bright host galaxies. Not surprisingly, we do find a corresponding (weak) correlation of optical luminosity and redshift for the sources in our sample. Another potential problem is the contamination of the host galaxy magnitude by nonthermal optical continuum radiation from the nucleus of the host galaxy, which might be expected to correlate with core radio power. Thus, the biases in

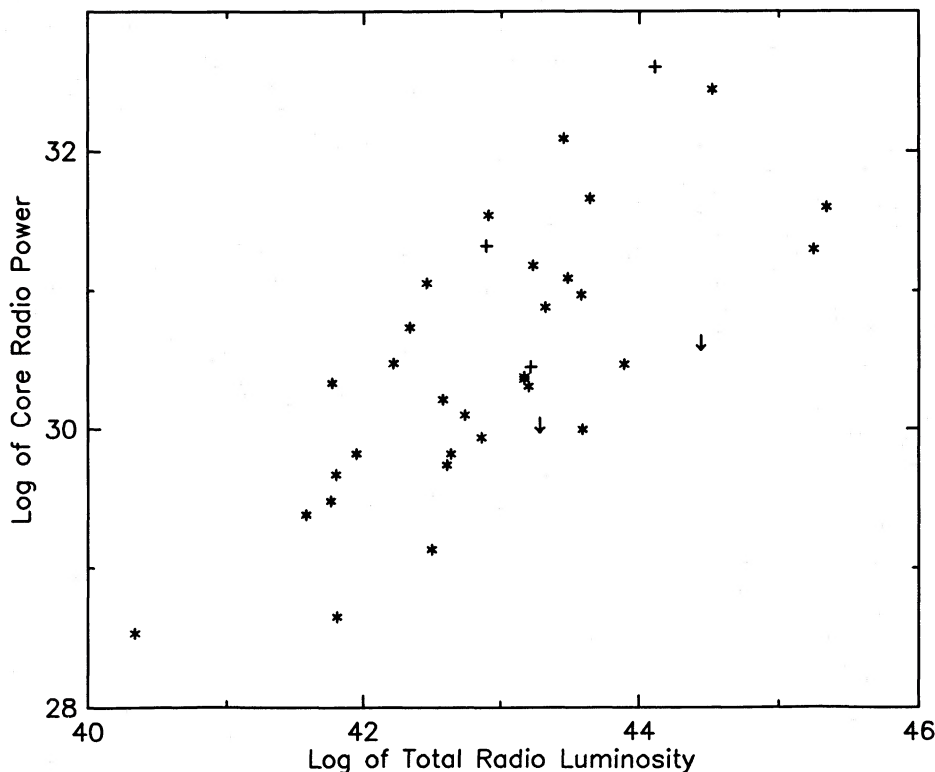


FIG. 5.—Plot of $\log_{10} P_{\text{radio core}}$ vs. $\log_{10} L_{\text{radio}}$, for the extended radio sources from the representative sample, where $P_{\text{radio core}}$ is the radio power of the core in $\text{ergs s}^{-1} \text{Hz}^{-1}$, and L_{radio} is the total radio luminosity in ergs s^{-1} . The broad line radio galaxies are indicated as crosses, and upper limits are indicated by arrows, where the midpoint of the arrow is located at the location of the limit.

our data set make it unsuitable for exploring the possible correlation of radio core power with optical continuum luminosity (Feretti *et al.* 1984; Ulrich and Meier 1984), or for examining the bivariate radio and optical luminosity function at high radio luminosities (e.g., Meier *et al.* 1979).

e) The Physical Parameters in the Very Extended Emission-Line Gas

We calculate lower limits to the density of the very extended ($r_{\text{gas}} \geq 5$ kpc) emission-line gas and upper limits to the mass of this gas (see Table 5) for a subset of the sources in our sample. Assuming case B recombination (i.e., that the nebula is optically thick to Lyman photons but optically thin to Balmer photons), the density in the emitting gas is given by

$$n_e^2 = \frac{L_{\text{H}\alpha}}{fV\alpha_{\text{H}\alpha}^{\text{eff}}h\nu_{\text{H}\alpha}},$$

where $L_{\text{H}\alpha}$ is the H α luminosity from the portion of the nebula for which the density is being estimated, V is the volume occupied by the emitting gas, f is the volume filling factor in the gas, h is Planck's constant, and $\nu_{\text{H}\alpha}$ is the frequency of the H α line. To calculate the density, we use the flux in a filament, at a distance r (given in col. [3] of Table 5) from the galaxy nucleus and take $\alpha_{\text{H}\alpha}^{\text{eff}} = 1.17 \times 10^{-13} \text{ cm}^3 \text{ s}^{-1}$ (Osterbrock 1974). For a filament of projected width w and length l , we assume a three-dimensional volume, $V = w^3/2l^{3/2}$. The values of n_e listed in column (2) of Table 5 assume a filling factor $f = 1.0$ and are, therefore, lower limits to the density. These values range from ~ 0.1 to 1 cm^{-3} at distances of 5–10 kpc from the galaxy nucleus.

We can estimate upper limits to the mass of emission-line gas, assuming case B recombination, from the relation

$$M_{\text{gas}} = fVn_e m_p = \frac{L_{\text{H}\alpha} m_p}{\alpha_{\text{H}\alpha}^{\text{eff}} h\nu_{\text{H}\alpha} n_e},$$

TABLE 5
LIMITS ON THE PHYSICAL CONDITIONS IN THE VERY EXTENDED EMISSION-LINE GAS

Source (1)	n_e (cm^{-3}) (2)	r (kpc) (3)	U (4)	M_{gas} (M_{\odot}) (5)
3C 63*	≥ 0.1	10	$\leq 1 \times 10^{-2}$	$\leq 6 \times 10^9$
PKS 0349–278*	≥ 0.1	10	$\leq 3 \times 10^{-3}$	$\leq 2 \times 10^9$
3C 98*	≥ 0.1	6	$\leq 3 \times 10^{-3}$	$\leq 8 \times 10^7$
PKS 0634–206*	≥ 0.1	20	$\leq 3 \times 10^{-4}$	$\leq 3 \times 10^9$
3C 171	≥ 0.2	10	$\leq 1 \times 10^{-2}$	$\leq 5 \times 10^9$
3C 192*	≥ 0.05	10	$\leq 8 \times 10^{-3}$	$\leq 8 \times 10^8$
3C 218*	≥ 0.2	5	$\leq 3 \times 10^{-3}$	$\leq 4 \times 10^7$
3C 223*	≥ 0.4	10	$\leq 4 \times 10^{-2}$	$\leq 3 \times 10^8$
3C 227*	≥ 0.1	10	$\leq 8 \times 10^{-2}$	$\leq 4 \times 10^9$
3C 274*	≥ 0.3	2	$\leq 4 \times 10^{-4}$	$\leq 3 \times 10^5$
3C 285	≥ 0.1	10	$\leq 2 \times 10^{-2}$	$\leq 1 \times 10^9$
3C 305	≥ 0.5	5	$\leq 6 \times 10^{-3}$	$\leq 1 \times 10^9$
3C 317*	≥ 0.1	5	$\leq 3 \times 10^{-3}$	$\leq 1 \times 10^8$
3C 321	≥ 0.2	10	$\leq 1 \times 10^{-2}$	$\leq 1 \times 10^9$

Col. 1.—Source name. An asterisk signifies membership in the representative sample.

Col. 2.—Lower limit to the density in the line-emitting gas at a distance r (given in col. [3]) from the galaxy nucleus.

Col. 3.—Radius at which the density and ionization parameter are calculated.

Col. 4.—Upper limit to the ionization parameter (U) in the gas at a distance r from the galaxy nucleus, assuming photoionization by a nonthermal continuum from the nucleus. See text for more details.

Col. 5.—Upper limit to the mass in emission-line gas. See text for details.

where $L_{\text{H}\alpha}$ is the total H α luminosity of the gas. We take $\alpha_{\text{H}\alpha}^{\text{eff}} = 1.17 \times 10^{-13} \text{ cm}^3 \text{ s}^{-1}$ (Osterbrock 1974) and use our lower limits to n_e , calculated assuming a filling factor of unity, to calculate an upper limit to the mass of emission-line gas. Since the emission-line gas near the nucleus of the galaxy is known to have very high densities ($\geq 10^{2.5} \text{ cm}^{-3}$; Koski 1978), we have not included the line luminosity which comes from gas within 5 projected kpc of the nucleus when calculating the mass of the emitting gas. We estimate upper limits to the mass in emission-line gas between 5×10^7 to $5 \times 10^9 M_{\odot}$. The actual mass of emission-line gas is directly proportional to the filling factor of the emission-line gas.

III. DISCUSSION

a) Confinement of the Emission-Line Nebulae

In the absence of a confining medium, the emission-line filaments will expand at their sound speed, and in roughly a sound crossing time, will no longer be visible. Thus, if the sound crossing time is short, compared to say the radio source lifetime, then we would not expect to find extended emission-line filaments preferentially associated with powerful radio sources unless the filaments were continually created.

We can estimate the lifetime of an emission-line region against expansion as $t_{\text{exp}} = d/c_s$, where d is the depth of the emitting region and c_s is the isothermal sound speed in the gas ($\sim 10 \text{ km s}^{-1}$ for gas at $T = 10^4 \text{ K}$). We can express d in terms of the ionizing flux intercepted by the filament and the density in the filament as follows. Assuming case B recombination, and approximating the emitting region as a plane parallel slab with cross-section area A , depth d , and distance from the central ionizing source r , we have

$$\frac{QA}{4\pi r^2} = A dn_{\text{H}} n_e \alpha_{\text{B}},$$

where Q is the number of ionizing photons per second emitted by the active nucleus, $QA/4\pi r^2$ is the fraction of the nuclear ionizing flux intercepted by the filament, and α_{B} is the case B hydrogen recombination coefficient, taken to be $2.6 \times 10^{-13} \text{ cm}^3 \text{ s}^{-1}$ (Osterbrock 1974).

Taking Q and n_e at a distance of 10 kpc from the galaxy nucleus, as given in Table 5, and assuming $n_{\text{H}} = n_e$, we estimate values of d between 1 and 6 kpc, typical of the two-dimensional projected sizes of the emission-line filaments. The corresponding expansion time scales are between 10^8 and $6 \times 10^8 \text{ yr}$. These time scales can be compared with a recombination time in the emission-line gas ($t_{\text{recomb}} \sim 10^5 n_e^{-1}$) of 10^5 – 10^6 yr , a cooling time for the emission-line gas ($t_{\text{cool}} \sim 1.5 \times 10^4 n_e^{-1}$) of 10^4 – 10^5 yr , and a canonical lifetime for radio sources of $\sim 10^7$ – 10^9 yr (e.g., Schmidt 1966; Cordey 1986). We note, however, that the expansion time scale is proportional to n_e^{-2} , and we have used the lower limits to the density in the emission-line gas, calculated assuming a filling factor of unity; if the filling factor of the extended emission-line gas is substantially less than unity, then the expansion time scale will decrease accordingly.

It is now known that many elliptical galaxies which are not at the centers of clusters have their own X-ray coronae, extending in most cases beyond the stellar light distribution and in some cases as far as 65 kpc from the galaxy nucleus (e.g., Forman, Jones, and Tucker 1985). If such X-ray coronae are present in the "isolated" radio galaxies in our sample, then this hot gas should provide pressure confinement for the very

extended emission-line gas, since in no case do we find emission-line gas at distances greater than $\sim 50 \text{ kpc}$ from the host galaxy nucleus. The models of Sarazin and White (1987) predict that, for isolated galaxies of similar absolute magnitude to the radio galaxies in our sample, the pressures in the X-ray halos at distances of $\sim 10 \text{ kpc}$ from the galaxy nucleus should be $P/k \sim 10^3$ – 10^4 K cm^{-3} , in rough agreement with the pressures we estimate in the emission-line gas, assuming densities of 0.1 – 1 cm^{-3} and a temperature of 10^4 K . As discussed in Paper III, the very extended emission-line gas may also be in pressure equilibrium with the radio source plasma.

Thus, if the filling factor in the very extended emission-line gas (i.e., the gas at distances $\geq 5 \text{ kpc}$ from the nucleus) is not too different from unity, then this gas is probably pressure confined by a hot ($T \sim 10^7 \text{ K}$), diffuse interstellar medium. However, even in the absence of a confining medium, if the filling factor of the gas is near unity, the lifetime of the emission-line filaments against expansion is roughly equal to the age of the radio source. Thus, these emission-line filaments may not need to be continuously created to be observed preferentially in association with powerful radio galaxies (although they do need to be continually ionized/heated).

b) Ionization of the Emission-Line Gas

We consider whether the data are consistent with a scenario in which the dominant source of ionization of both the nuclear and the extended emission-line gas is a nuclear ionizing continuum.

The nuclear, nonstellar optical continuum is strongly correlated with the H β emission-line luminosity in powerful radio galaxies (Yee and Oke 1978). This correlation can be easily understood if the emission-line gas is photoionized by isotropically emitted radiation from the active nucleus of the host galaxy. Other explanations are, of course, also possible. For instance, the infall of ionized gas may provide the fuel for the central engine, or the emission-line luminosity and the strength of the nonstellar nuclear continuum may be independently correlated with a third parameter.

For some of the sources in our sample, estimates of the nonstellar, nuclear continuum flux are available in the literature. For these sources we can determine whether the nuclear ionizing continuum is sufficient to ionize the full extent of the emission-line nebulae we observe. We first calculate the total number of photons needed to photoionize the emission-line nebulae. We assume that the narrow emission-line gas is optically thick to Lyman photons but is optically thin to Balmer photons (case B recombination). Under these conditions, for gas at 10^4 K , $\sim 45\%$ of all Balmer photons will emerge from the nebula as H α photons (Osterbrock 1974). Then, using the Zanstra method (Zanstra 1931), we can relate the total H α luminosity of the emission-line gas to the total number of photons with energies greater than 13.5 eV needed, per second, to ionize the entire nebula:

$$Q_{\text{tot}} = \frac{2.2L_{\text{H}\alpha}}{h\nu_{\alpha}} \text{ photons s}^{-1},$$

where $L_{\text{H}\alpha}$ is the H α luminosity of the entire nebula. Since our emission-line images contain emission from either H α and [N II], or [O III], we assume line ratios of [O III]/H α = 3.8, and ([N II] λ 6584 + [N II] λ 6548)/H α = 1.2, in order to estimate the luminosity in H α alone (e.g., Koski 1978). For the sources with broad emission lines, we assume that the ratio of

TABLE 6
PHOTOIONIZATION PARAMETERS

Source (1)	Q_{tot} (2)	Q_{nuc} (3)	$Q_{\text{tot}}/Q_{\text{nuc}}$ (4)
3C 33*	1.7×10^{53}	1.7×10^{53a}	1.0
3C 78*	1.9×10^{52}	$< 1.1 \times 10^{53a}$	> 0.2
3C 88*	2.3×10^{52}	$< 6.4 \times 10^{52a}$	> 0.4
3C 98*	3.1×10^{52}	$< 1.3 \times 10^{53a}$	> 0.2
3C 171	1.6×10^{54}	7.4×10^{53a}	2.2
3C 192*	8.8×10^{52}	$\leq 9.9 \times 10^{52b}$	≥ 0.9
3C 219*	4.8×10^{53}	4.7×10^{53a}	1.0
3C 223*	3.5×10^{53}	$\leq 5.3 \times 10^{54b}$	≥ 0.1
3C 227*	1.2×10^{54}	1.9×10^{54a}	0.6
3C 264*	1.1×10^{52}	$< 2.3 \times 10^{52a}$	> 0.5
3C 272.1*	7.9×10^{50}	2.9×10^{51d}	0.3
3C 274*	6.6×10^{51}	3.3×10^{51c}	2.0
3C 285	1.4×10^{53}	2.5×10^{53a}	0.6
3C 305	2.7×10^{53}	2.2×10^{53a}	1.2
3C 321	3.9×10^{53}	$\leq 6.6 \times 10^{53b}$	≥ 0.6
3C 390.3*	1.8×10^{54}	3.2×10^{54a}	0.6
3C 405*	5.5×10^{53}	1.2×10^{54a}	0.5
3C 442*	1.2×10^{52}	$\leq 8.6 \times 10^{52b}$	≥ 0.1

Col. (1): Source name. An asterisk denotes membership in the representative sample.

Col. (2): Q_{tot} is the number of ionizing photons per second needed to ionize the entire emission-line nebula. See text for details.

Col. (3): Q_{nuc} is the number of ionizing photons per second emitted by the active nucleus. A superscript "a" indicates that Q_{nuc} is derived from an estimate of the nonthermal optical continuum as given by Yee and Oke 1978 or Yee 1980. A superscript "b" indicates the Q_{nuc} is derived from a total X-ray flux from Fabbiano *et al.* 1984, a superscript "c" that Q_{nuc} is derived from a measurement of the nuclear X-ray flux as given by Schreier, Gorenstein, and Feigelson 1982, and a superscript "d" that Q_{nuc} is derived from an ultraviolet flux as given by Hansen, Norgaard, Nielsen, and Jorgensen 1985. See text for details.

Col. (4): The ratio of cols. (2) and (3).

ionizing photons to H α photons is 0.45 (instead of 2.2), as given by Kwan and Krolik (1981), for the line emission which comes from the broad-line region. In column (2) of Table 6, we list the values of Q_{tot} derived in this way.

For 13 of the sources in our sample, estimates of the non-stellar flux from the galaxy nucleus in the wavelength band from 3000 to 9500 Å are available (Yee and Oke 1978; Yee 1980). For these sources, we calculate the total number of ionizing photons per second (Q_{nuc}) produced by the extension of the optical nonstellar flux into the ultraviolet. We assume the spectrum of the nonthermal nuclear radiation is given by $F_{\nu} \propto \nu^{\alpha}$, with $\alpha = -1$, and that the radiation is emitted isotropically.

For an additional three sources in our sample, X-ray luminosities from 1.5 to 3 keV are available (Fabbiano *et al.* 1984). The X-ray emission may come from the active nucleus of the galaxy, from the galaxy's ISM, or in some cases from an intergalactic medium. The observed X-ray luminosity is therefore an upper limit to the luminosity of the active nucleus. For M87, an estimate of the nuclear X-ray flux was available from Schreier, Gorenstein, and Feigelson (1982). Hansen, Norgaard-Nielsen, and Jorgensen (1985) reported an ultraviolet flux (at 1510 Å) for M84. In all cases we calculate Q_{nuc} (the total number of ionizing photons produced by the active nucleus), assuming isotropic emission of power-law radiation from the active nucleus with a slope of $\alpha = -1$.

The values of Q_{nuc} calculated in this way are given in column (3) of Table 6. They are, of course, only estimates of the number

of ionizing photons emitted per second by the active nucleus, since, in actuality, we know neither the strength or the shape of the ionizing continuum. In column (4), we give the ratio $Q_{\text{tot}}/Q_{\text{nuc}}$, and in Figure 6, we plot Q_{tot} versus Q_{nuc} . For the radio galaxies in our sample, we find that Q_{tot} correlates strongly with Q_{nuc} (where the probability that the two are uncorrelated is 5×10^{-6} , using a generalized Kendal tau test), and we determine values for the ratio of Q_{tot} to Q_{nuc} (sometimes termed the covering factor) of between 0.1 and 2 with a median value of ~ 0.5 . Figure 6 also shows, superposed with the radio galaxies, the radio-loud, steep-spectrum QSOs from the sample of Stockton and MacKenty (1987).⁸ The radio-loud, steep-spectrum QSOs extend the relationship found for the radio galaxies an additional order of magnitude in each parameter.

We can also calculate a lower limit to the flux of ionizing photons emitted by the active nucleus, using an alternate method. Assuming the ionizing radiation is emitted isotropically from the galaxy nucleus,

$$Q_{\text{nuc, min}} = \frac{4\pi Q_{\text{neb}}}{\Omega},$$

where Q_{neb} is the number of photons per second needed to ionize any portion of the nebula and Ω is the solid angle intercepted by that portion of the nebula. We find that, for the sources from the representative sample, $Q_{\text{nuc, min}}$ is in almost all cases, less than or comparable to Q_{tot} , the total number of ionizing photons needed to ionize the entire nebula. This is understandable, since in most of these sources a significant fraction of the total emission-line luminosity comes from a symmetric appearing region of gas near the galaxy nucleus (see § IIc[ii]).

Assuming that the emission-line nebulae are photoionized by the nonthermal nuclear continuum, we use our lower limits to the density and our estimates of Q_{nuc} to calculate upper limits to the ionization parameter ($U = Q_{\text{nuc}}/4\pi r^2 n_e c$) in the emission-line gas. We assume $Q_{\text{nuc}} = Q_{\text{tot}}$ for those sources where no estimate of Q_{nuc} is available. Under these assumptions, we estimate upper limits for U of $\sim 5 \times 10^{-2}$ – 5×10^{-4} at distances between 5 and 10 kpc from the galaxy nucleus (see col. [4] of Table 5), typical of the ionization parameters found for the narrow line regions of the Seyfert 2 galaxies and LINERS (e.g., Ferland and Netzer 1983).

Thus, for the galaxies in our sample where the requisite information was available, we find, in all cases, that the nuclear continuum is roughly sufficient to photoionize the full extent of the observed emission-line nebula. We also find that the number of ionizing photons emitted by the active nucleus (Q_{nuc}) is strongly correlated with (and roughly twice) the number of photons which are needed to photoionize the observed emission-line nebulae (Q_{tot}). Recently, Robinson *et al.* (1987) have obtained diagnostic emission-line ratios for the extended narrow emission-line gas in a sample of 11 powerful radio galaxies. They find that, in most cases, the ionization states of both the nuclear and the off nuclear emission line gas are consistent with a model in which the gas is photoionized by a single continuum, but over a range in ionization parameter. These results are most easily understood within the context of

⁸ We have calculated Q_{nuc} from the optical continuum at H β assuming a power-law spectrum with slope minus one, and Q_{tot} from the broad H β nuclear flux assuming that the ratio of ionizing photons to broad H β photons is 2.5 (Kwan and Krolik 1981) and from the extended [O III] flux as for the radio galaxies.

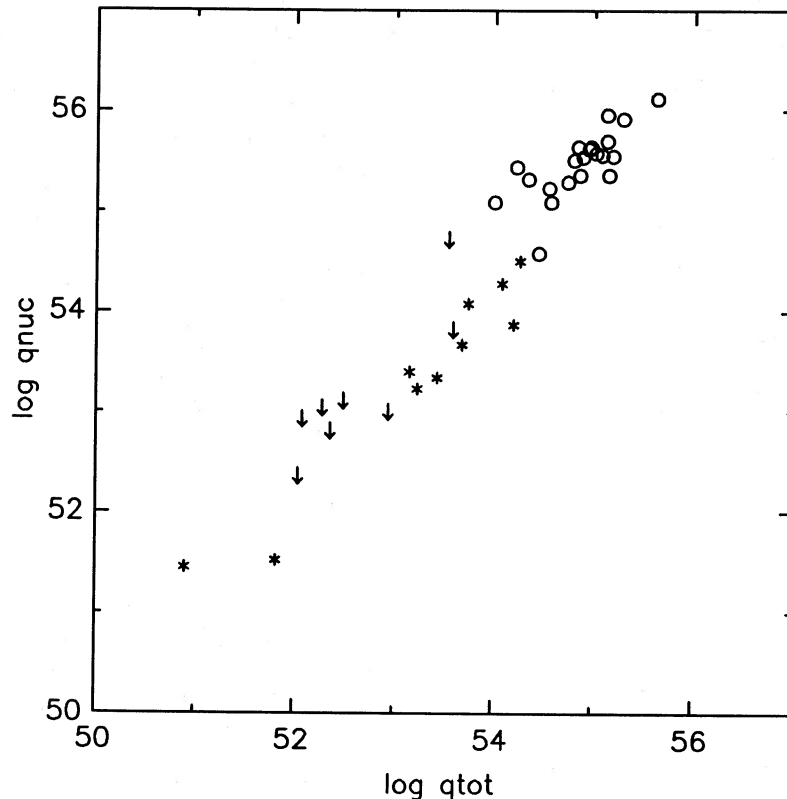


FIG. 6.—Plot of $\log_{10} Q_{\text{nuc}}$ vs. $\log_{10} Q_{\text{tot}}$ for the sources from the representative and special samples for which the requisite information was available, Q_{nuc} is the number of ionizing photons emitted by the galaxy nucleus, and Q_{tot} is the total number of photons needed to ionize the observed emission-line nebula. Open circles signify the steep-spectrum, radio-loud QSOs from Stockton and MacKenty (1987).

a model in which photoionization by a nuclear continuum is the dominant means by which the nuclear and extended emission-line gas is ionized.

In such a model, the emission-line luminosity of a powerful radio galaxy should be determined by the flux of ionizing photons and the availability of hydrogen atoms. The strong correlation of Q_{nuc} with Q_{tot} suggests that the emission-line luminosities of the radio sources in our sample are determined primarily by the flux of ionizing photons emitted by the active nucleus (and see also Kinney *et al.* 1985). Thus, in general, the emission-line luminosity does not appear to be limited by the availability of cold gas (but see also Paper III). One interpretation of this result is that the covering factor of the nucleus by cold gas is roughly constant from source to source, and the individual emission-line clouds are ionization bounded (i.e., optically thick to the ionizing radiation). This suggests that there may be considerably more mass in neutral gas around the nuclei of radio galaxies than there is in ionized gas. In this regard we note that Golombek, Miley, and Neugebauer (1988) found that (1) the most powerful radio galaxies in their sample of 131 radio galaxies were strong far-infrared sources, (2) large infrared emission in radio galaxies is correlated with the presence of strong emission lines in the optical spectra, and (3) interstellar dust is the likely source of the bulk of the far-infrared emission observed in radio galaxies.

Further, high spatial resolution observations of the 21 cm line in absorption against the bright-spatially resolved radio source in NGC 5128 (Centaurus A) provide strong evidence that there is neutral hydrogen within ~ 200 pc of the nucleus in

this radio galaxy (van der Hulst, Golisch, and Haschick 1983).

An alternate explanation for the strong correlation of Q_{nuc} with Q_{tot} is that the availability of hydrogen atoms is independently correlated with the continuum luminosity of the active nucleus. For example, infalling cold gas may fuel the central engine. The number of available hydrogen atoms would need to rise roughly directly with the number of ionizing photons to explain the observed slope near unity in the relationship between $\log Q_{\text{nuc}}$ and $\log Q_{\text{tot}}$.

Thus, the evidence seems to suggest that photoionization by a nuclear ionizing source is the dominant means by which both the nuclear and the extended emission-line gas in powerful radio galaxies is ionized. This does not rule out the possibility that portions of the extended emission-line regions in some sources are locally photoionized by young, hot stars mixed with the emission-line gas. However, Robinson *et al.* (1987) concluded that the line ratios found in the very extended emission-line gas in the (low to moderate redshift) radio sources which they have observed are inconsistent with those expected for photoionization by typical O and B stars. It is also possible, that in some instances the radio source is directly, or indirectly, involved in ionizing the gas. This possibility will be discussed in detail in Paper III. Finally, we note that while photoionization by the active nucleus appears to dominate the ionization of the emission-line gas in moderate to high power radio sources, Wilkinson *et al.* (1980) have suggested that an alternate source of ionization, such as collisional ionization from shocks, may provide an important source of ionization in low-power radio galaxies ($L_{\text{radio}} \lesssim 10^{42}$ ergs s^{-1}).

c) *The Origin of the Emission-Line Gas*

We consider two possible origins for the emission-line gas: (1) thermal instabilities in a hot, diffuse interstellar or intergalactic medium and (2) tidal interactions (or mergers) with companion galaxies. We discuss each of these in turn.

i) *Thermal Instabilities in a Hot, Diffuse Medium*

In some clusters of galaxies, the bremsstrahlung cooling time of the hot gas in the cluster core is less than the age of the cluster. If heating and thermal conduction are not fully effective in resupplying the energy lost through the radiative cooling of the gas (Lea and Holman 1978; Tucker and Rosner 1983; Miller 1986; Bertschinger and Meiksin 1986; Rephaeli 1987), then some amount of gas should be cooling and falling into the center of the cluster potential (e.g., Fabian, Nulsen, and Canizares 1984; Stewart *et al.* 1984; Sarazin 1986, and references therein). The detection of optical emission-line filaments in a dozen or more galaxies at the centers of such "cooling flow" clusters (Heckman 1981; Cowie *et al.* 1983; Hu *et al.* 1985; Johnstone, Fabian, and Nulsen 1987) has been taken as supporting evidence that these clusters possess cooling flows (but see also Nulsen 1986; Baum and Heckman 1987).

Some of the radio sources in our sample are known to be associated with galaxies at the centers of clusters and with groups of galaxies (see Paper I). For some of these sources, the bremsstrahlung cooling time of the hot intergalactic gas surrounding the radio galaxy has been shown to be less than the age of the universe (e.g., PKS 0745–191, 3C 218, 3C 274, 3C 295, 3C 317, 3C 405). In clusters and groups of galaxies, the reservoir of cooling gas is large ($M_{\text{gas}} \sim 10^{12} M_{\odot}$ within 0.5 Mpc, in clusters), as is the size scale of the cooling region ($r_{\text{cool}} \sim 100$ kpc) (Stewart *et al.* 1984). Thus, for the sources in our sample which are known to be associated with galaxies at the centers of clusters or groups it is quite possible that the gas we observe in emission lines has cooled out of a surrounding hot intergalactic medium.

While some of the sources in our sample which have extensive emission-line filaments appear to be members of groups or clusters of galaxies, others inhabit much more isolated environments (e.g., 3C 98, PKS 0634–206, 3C 192, 3C 227). There is, at present, no evidence for the existence of an intergalactic medium with a short cooling time around these galaxies. However, many large elliptical galaxies which are not at the centers of clusters are known to possess X-ray halos of their own. The cooling time of the hot ($T \sim 10^7$ K) interstellar medium in the X-ray coronae of these galaxies is typically short ($t_{\text{cool}} \lesssim 10^9$ yr; e.g., Forman, Jones, and Tucker 1985; Thomas *et al.* 1986), and thermal instabilities are expected to form in the cooling gas. Cooling and the formation of thermal instabilities are expected to be most important within one core radius of the galaxy nucleus ($\lesssim 1$ kpc for isolated ellipticals) (White and Chevalier 1984; Nulsen, Stewart, and Fabian 1984; Sarazin and White 1987). Indeed, thermally unstable filaments in the hot ISM have been suggested as a likely origin of the small ($\lesssim 1$ kpc) emission-line regions found in the centers of normal elliptical galaxies (Demoulin-Ulrich, Butcher, and Boksenberg 1984; Phillips *et al.* 1986), and may also be the source of some of the smaller regions of emission-line gas found in some of the radio galaxies in our sample.

However, the large (10–100 kpc), and coherent, emission-line filaments seen in some of the isolated galaxies in our sample (for instance, those in 3C 192, or 3C 227) seem unlikely to have

originated from thermal instabilities in a cooling flow in the ISM of an isolated elliptical galaxy. These filaments show coherent structure on the size-scale of the galaxy, and there is no obvious morphological connection between the distribution of this emission-line gas and the stellar continuum light. However, it is possible that the radio source has redistributed cold gas from the inner portions of the galaxy or induced instabilities in the hot interstellar medium at large distances from the host galaxy nucleus (see Paper III).

In some of these isolated radio galaxies, we estimate upper limits to the mass in emission-line gas of several times $10^9 M_{\odot}$. Unless the actual mass in emission-line gas is significantly less than our limits, this would represent a substantial fraction of the mass in the hot component of the ISM, and a substantial fraction of the total mass that is expected to have cooled out of the hot ISM (assuming mass accretion rates between 0.02 and $3 M_{\odot} \text{ yr}^{-1}$ for isolated elliptical galaxies; Thomas *et al.* 1986). Most of the mass accreted from the hot component of the ISM is expected to return to the stellar population as the gas cools through 10^4 K, becomes atomic and/or molecular, and undergoes star formation. Thus, if there really is $\sim 10^9 M_{\odot}$ of material in emission-line gas within the ISM of an isolated elliptical galaxy, it is not likely to have originated from instabilities in the hot ISM. However, we note that where it has been possible to estimate densities in extended optical emission-line gas through the detection of the S II lines (e.g., in the bright emission-line nebula associated with central dominant galaxies in cluster cooling flows), the total mass in emission-line gas has been found to be $M_{\text{gas}} \lesssim 10^6 M_{\odot}$ (Hu *et al.* 1985; Heckman *et al.* 1989).

ii) *Mergers and Tidal Interactions*

The role of tidal interactions and mergers in stimulating activity in powerful radio galaxies and quasars has received ever increasing attention in recent years (e.g., Heckman *et al.* 1986; Hutchings 1987; Schweizer 1986). We are interested in considering whether there is evidence that the extended emission-line gas we observe has been acquired in tidal interactions or mergers with companion galaxies. We therefore consider whether there is independent evidence that some of the galaxies in our sample are engaged or have been engaged in galaxy-galaxy interactions.

Toomre and Toomre (1972), Toomre (1977), and Quinn (1984) have shown that mergers and tidal interactions can produce a wide range of distortions in the distribution of the starlight, ranging from tails and fans, to shells, depending on the impact parameter of the encounter, the viewing angle of the observer, and the nature of the merger participants (e.g., the presence of a dynamically cold component and the relative masses of the participants). Thus, distortions of the stellar isophotes of the host galaxy can be signs of a recent interaction, as can secondary nuclei, bridges of gas between two galaxies, and, possibly, the presence of a dust lane.

We consider only the 33 sources from the representative sample at redshifts less than 0.3, since at higher redshifts our ability to detect morphological peculiarities in the distribution of the optical continuum light is greatly reduced (see also Heckman *et al.* 1986). We separate the sources into five groups. In the nine Group I sources (3C 33, 3C 98, PKS 0634–206, 3C 223, 3C 272.1, PKS 1345+125, 3C 327, 3C 403, 3C 405), the optical (continuum) isophotes of the host galaxies show either clear signs of morphological disturbance or a dustlane. In the six Group II sources (PKS 0745–191, 3C 196.1, 3C 218, 3C

TABLE 7
INTERACTING AND NONINTERACTING GALAXIES

Category (1)	L_{radio} (2)	L_{lines} (3)	$100L_{\text{lines}}$			Number (7)
			L_{radio} (4)	d_{neb} (5)	d_{radio} (6)	
Group I	1.5×10^{43}	9.9×10^{41}	3.5	11.1	213	9
Group II	2.2×10^{43}	3.6×10^{41}	2.1	14.0	38	6
Group III	2.2×10^{43}	1.0×10^{42}	8.6	43.0	170	2
Group IV	6.2×10^{41}	2.7×10^{42}	2.2	3.0	162	6
Group V	5.9×10^{42}	7.4×10^{40}	1.7	4.2	141	10
Groups I, II, and III	1.8×10^{43}	4.6×10^{41}	3.5	13.7	125	17
Groups IV and V	3.4×10^{42}	4.8×10^{40}	1.9	3.9	130	16

Col. (1): Category of host galaxy. See text for details.

Col. (2): Median radio luminosity in ergs s^{-1} .

Col. (3): Median line luminosity in ergs s^{-1} .

Col. (4): Median ratio of $\text{H}\alpha + \text{N II}$ luminosity to the radio luminosity.

Col. (5): Median diameter of emission line nebula, in kpc.

Col. (6): Median extent of radio source, in kpc.

Col. (7): Number of sources in that category.

227, 3C 317, 3C 346), the host galaxy has a potential (unresolved) secondary nucleus within 15 kpc of the primary nucleus. In the two Group III, sources, a bridge emission-line gas connects the radio galaxy to a nearby (in projection) galaxy. This group contains only the sources 3C 63 and PKS 0349–278. The emission-line gas in both these sources is distributed in an S-shape. S-shaped emission-line regions can be interpreted as either bridge tail systems (Toomre and Toomre 1977) or warped disks of gas seen edge on. Several authors (e.g., Tubbs 1980; van Albada, Kotanyi, and Schwarzschild 1982) have suggested that captured gas settling into the potential of an elliptical galaxy will assume such a distribution. In the six group IV sources (3C 40, 3C 75, 3C 264, 3C 278, 3C 433, 3C 442), a second elliptical galaxy (of comparable size to the radio galaxy) is projected within the stellar envelope of the radio galaxy. In these dumbbell galaxies the potential interaction involves two elliptical galaxies, neither of which is likely to rich in cold gas. Finally, the 10 group V sources (3C 29, 3C 78, 3C 88, 3C 89, 3C 105, 3C 192, 3C 219, 3C 274, 3C 353, 3C 390.3) show no obvious signs of an interaction.

We wish to determine whether there are differences in the emission-line and radio properties of the “interacting galaxies” and the “noninteracting galaxies.” In Table 7, for each of the five groups and for the combined sources from groups I, II, and III, and groups IV and V, we have tabulated the median radio luminosity, line luminosity, ratio of line to radio luminosity, radio source size, and emission-line nebula size.

All of the groups have similar ratios of line to radio luminosity. We find that the “dumbbell galaxies” (group IV sources) have the lowest median L_{radio} , L_{lines} , and the smallest median d_{neb} . By contrast, the other sources which show signs of an interaction, the sources from groups I, II, and III, have the highest median L_{line} , L_{radio} , and largest median d_{neb} . The differences in the median line and radio luminosities for the group IV galaxies and the combined group I, II, and III galaxies are not statistically significant; however, the difference in the median size of the emission-line nebulae are. In Figure 7, we show the distribution of d_{neb} for the “interacting galaxies” (combined groups I, II, and III sources), the dumbbell (or group IV) galaxies, and the “undisturbed” (group V) galaxies. Applying a Kolmogorov-Smirnov two-sample test (Smirnov 1939;

Conover 1980), we find that the difference between the distributions of d_{neb} are significant at greater than the 99% confidence level, using a two-sided test.

Thus, we find that, excluding the dumbbell galaxies, galaxies which show potential evidence that they are undergoing or have recently been involved in an interaction have emission-line nebulae which are more extended than their “noninteracting” counterparts. One possible explanation of this result is that the emission-line gas has been acquired during an interaction with a gas-rich companion, since in that case we might expect galaxies which are presently interacting or which have recently undergone an interaction to show more extensive, disordered emission line regions.

However, several caveats are in order. First, of the six potential multiple nuclei galaxies, three are known to be at the centers of clusters of galaxies, and an additional two appear to inhabit galaxy-rich environments. As discussed above, the emission-line gas associated with galaxies in such rich environments may cool out of the hot intergalactic medium, although mergers/interactions do also occur in these environments. Second, it is also possible that the mergers and tidal interactions have simply “stirred up” and redistributed cold gas which was present in the host galaxy prior to the interaction. Third, the radio source may play an important role in determining the distribution of the emission-line gas (see Paper III).

It is not clear why the dumbbell galaxies have the lowest median values of d_{neb} , L_{radio} , and L_{line} (note that these three quantities are correlated with one another). All of the dumbbell galaxies are located in cluster environments. As discussed above, the emission-line gas which is found in galaxies in rich environments may be accreted from the ICM. It is possible that the presence of a dumbbell galaxy (i.e., of two dominant galaxies in orbit) is indicative of a condition, such as the merging of two subclusters, which is inhibitory to the formation of a cooling accretion flow in the ICM.

IV. SUMMARY

In this paper, we present the statistical results of a program of optical and radio observations of a representative sample of radio galaxies conducted in order to study the optical

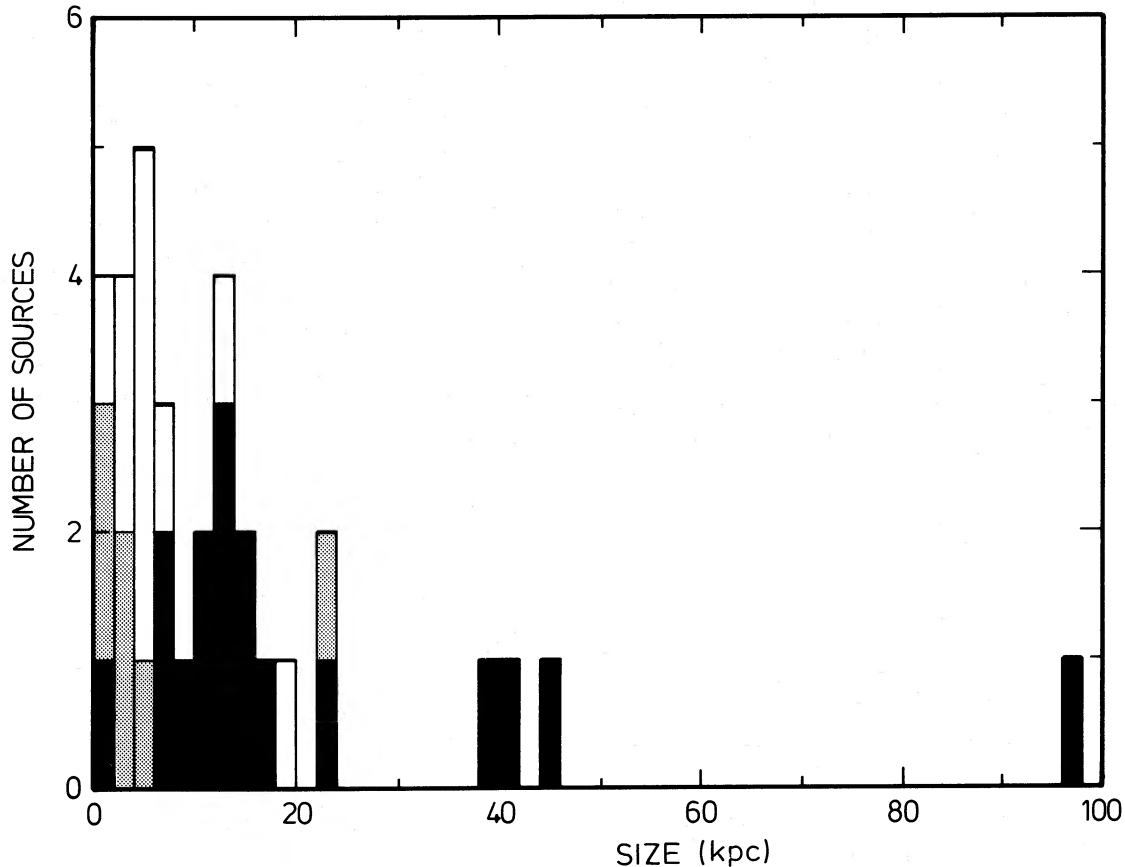


FIG. 7.—Histogram of d_{neb} , the extent of the emission-line nebula in kiloparsecs, for the sources in the representative sample with $z < 0.3$. The shading denotes the classification of the host galaxy as described in the text, where the potentially interacting galaxies from groups I, II, and III are shaded black, the dumbbell galaxies from group IV are shaded gray, and the “noninteracting” galaxies from group V are unshaded.

emission-line properties of powerful radio galaxies. We find the following results:

1. We establish that spatially extended emission-line gas is common in powerful radio galaxies. We detect line emission from all of the sources in the representative sample. In $\sim 85\%$ of these sources we have resolved the line emission. The median extent of the emission-line nebulae is 10 kpc, and the median emission-line luminosity in $\text{H}\alpha + [\text{N II}]$ or $[\text{O III}]$ is 3×10^{41} ergs s^{-1} , roughly an order of magnitude times the extent and luminosity of emission line nebulae in normal early-type galaxies of similar optical magnitude.

2. The emission-line nebulae in the sources in the representative sample span a range in extent and morphology. In some sources we observe only small, centrally condensed, kiloparsec scale regions of line emission, while in others we detect much more extensive filaments of line emitting gas tens of kiloparsecs from the host galaxy nucleus. The small emission-line nebulae are typically centered on and roughly symmetric about their host galaxy nuclei, and they often have roughly “elliptical” or “oval” shapes. In contrast, in the sources from the representative sample with larger emission-line nebulae, the line emission tends to be filamentary in appearance, and the very extended line-emitting gas in these sources is typically asymmetrically distributed with respect to the host galaxy nucleus.

3. The median extent of the emission line nebulae in sources with edge-dimmed, FR1 radio morphologies, or with total radio luminosities less than $10^{42.7}$ ergs s^{-1} , is roughly one-

fourth the median extent in sources with edge brightened, FR2, and amorphous radio morphologies, or total radio luminosities greater than $10^{42.7}$ ergs s^{-1} . The larger median size of the nebulae in the more powerful sources may reflect (1) the increased ionizing capability of the central engine, (2) an interaction of the radio source with the emission line gas (see Paper III), or (3) differing origins for the emission-line gas in the low- and high-power radio galaxies (e.g., Heckman *et al.* 1986).

4. We find very strong correlations of the emission-line luminosity with both the total radio luminosity and the core radio power for the sources from the representative sample, as well as a strong correlation of the total and core radio powers.

5. We estimate lower limits to the density of the emission-line gas at distances between 5 and 10 kpc from the galaxy nucleus of 10.1 to 1 cm^{-3} , and upper limits to the total mass in emission-line gas between 5×10^7 and $5 \times 10^9 M_{\odot}$.

6. We argue that, if the filling factor in the very extended emission-line gas (i.e., the gas at distances ≥ 5 kpc from the nucleus) is not too different from unity, then the line-emitting gas may be in pressure equilibrium with a hot ($T \sim 10^7$ K), diffuse interstellar medium, but even in the absence of a confining medium, the lifetime of the emission-line filaments against expansion is roughly equal to the age of the radio source. Thus, the very extended emission-line filaments may not need to be continuously created to be observed preferentially in association with powerful radio galaxies (although they do need to be continually ionized/heated).

7. The number of photons required to photoionize the emission-line nebula (Q_{tot}) is found to correlate strongly with the number of ionizing photons emitted by the galaxy nucleus (Q_{nuc}), as estimated from measurements of the nuclear, "non-stellar" optical continuum from the host galaxy. Assuming the ionizing continuum is a power law with slope -1 (i.e., $F_{\nu} \propto \nu^{-1}$), we estimate that the ionizing continuum from the nucleus is sufficient, in the cases studied, to ionize the extended emission-line nebulae we observe. These results, combined with the spectroscopic and modeling results of Robinson *et al.* (1987), suggest that photoionization by the host galaxy's nuclear ultraviolet continuum is the *dominant* means by which both the nuclear and the extended emission-line gas in powerful radio galaxies is ionized. The strong correlation of Q_{tot} with Q_{nuc} suggests that the emission-line luminosities of powerful radio galaxies are determined by the strength of the nuclear ionizing continuum and not, in general, by the availability of cold gas.

8. We consider possible origins for the emission-line gas. Instabilities in the hot intergalactic medium of the host galaxy may be the source of the emission-line gas in sources which have small (i.e., kpc scale) emission-line nebulae. However, the large spatial extent of the emission-line nebulae in some very isolated galaxies and the possibly large associated masses in emission-line gas may suggest that these very extensive regions of emission-line gas do not originate in the ISMs of their host galaxies. For sources with very extended regions of emission-line gas which inhabit densely populated regions, the emission-line gas may, however, have cooled out of a hot *intergalactic* medium. We also consider the possibility that the emission-line gas in these radio galaxies originates in tidal interactions/

mergers with companion galaxies which are rich in cold gas. In support of this scenario, we find that the median extent of the emission-line nebulae is larger in galaxies which show possible signs of a recent interaction (e.g., optical continuum morphological peculiarities, a second nucleus, or a bridge of emission-line gas to a second galaxy) than in either dumbbell galaxies or galaxies which show no signs of a recent interaction. The interactions may either have supplied the cold gas or stirred up preexisting cold gas in the radio galaxy's ISM.

9. We find obvious morphological peculiarities in the optical continuum isophotes of $\sim 25\%$ of the galaxies from the representative sample (where we have not included galaxies in which the only signs of distortion is a radial change in the orientation or ellipticity of elliptical isophotes).

10. We find that there are roughly two orders of magnitude in radio luminosity separating the luminosity regime in which the sources in our sample have exclusively edge-darkened (Fanaroff and Riley Class I) radio morphologies from the regime in which sources have exclusively edge-brightened, hot-spotted (Fanaroff and Riley Class II) radio morphologies.

11. We find a tendency for the radio source axis to align with the minor axis of the host galaxy only in galaxies which have radio sources which are greater than 200 kpc in extent.

We acknowledge support from NSF grant AST85-15896 and thank Wil van Breugel, Alan Bridle, and George Miley for many scientific discussions. S. A. B. thanks NRAO for the award of a predoctoral research associateship, G. Kessler for his careful work on the figures, C. O'Dea for comments on the paper and encouragement, and little C. O'Dea and D. Mint for moral support.

REFERENCES

- Baars, J. W. M., Genzel, R., Pauliny-Toth, I. I. K., and Witzel, A. 1977, *Astr. Ap.*, **61**, 99.
- Baum, S. A., and Heckman, T. M. 1987, in *Radio Continuum Processes in Clusters of Galaxies*, ed. C. P. O'Dea and J. M. Uson (Greenbank: NRAO), p. 119.
- . 1989, *Ap. J.*, **336**, 702 (Paper III).
- Baum, S. A., Heckman, T. M., Bridle, A. H., van Breugel, W., and Miley, G. K. 1988, *Ap. J. Suppl.*, **68**, 833 (Paper I).
- Bertschinger, E., and Meiksin, A. 1986, *Ap. J. (Letters)*, **306**, L1.
- Biretta, J. A., Owen, F. N., and Hardee, P. E. 1983, *Ap. J. (Letters)*, **274**, L27.
- Bridle, A. H., Perley, R. A., and Henriksen, R. N. 1986, *A. J.*, **92**, 534.
- Burstein, D., and Heiles, 1982, *A. J.*, **87**, 1165.
- Chambers, K. C., Miely, G. K., and van Breugel, W. 1987, *Nature*, **329**, 606.
- Cohen, R. D., and Osterbrock, E. 1981, *Ap. J.*, **243**, 81.
- Colla, G., *et al.* 1973, *Astr. Ap. Suppl.*, **11**, 291.
- Conover, W. J. 1980, *Practical Nonparametric Statistics* (New York: Wiley).
- Cordey, R. A. 1986, *M.N.R.A.S.*, **219**, 575.
- Costero, R., and Osterbrock, D. E. 1977, *Ap. J.*, **211**, 675.
- Cowie, L. L., Fabian, A. C., and Nulsen, P. E. J. 1980, *M.N.R.A.S.*, **191**, 399.
- Cowie, L. L., Hu, E. M., Jenkins, E. B., and York, D. G. 1983, *Ap. J.*, **272**, 29.
- Danziger, I. J., Fosbury, R. A. E., Goss, W. M., Bland, J., and Boksenberg, A. 1984, *M.N.R.A.S.*, **208**, 589.
- Demoulin-Ulrich, M.-H., Butcher, H. R., and Boksenberg, A. 1984, *Ap. J.*, **285**, 527.
- Ebeneter, K., Djorgovski, S., and Davis, M. 1988, *A. J.*, **95**, 422.
- Ekers, R., and Simkin, S. 1983, *Ap. J.*, **265**, 85.
- Elsmore, B., and Mackay, C. D. 1969, *M.N.R.A.S.*, **146**, 361.
- Fabbiano, G., Miller, L., Trinchieri, G., Longair, M., and Elvis, M. 1984, *Ap. J.*, **277**, 115.
- Fabian, F. C., Nulsen, P. E. J., and Canizares, C. R. 1984, *Nature*, **310**, 733.
- Fanaroff, B. L., and Riley, F. M. 1974, *M.N.R.A.S.*, **167**, 31P.
- Feretti, L., Giovannini, G., Gregorini, L., Parma, P., and Zamorani, G. 1984, *Astr. Ap.*, **139**, 55.
- Ferland, G. J., and Netzer, H. 1983, *Ap. J.*, **264**, 105.
- Forman, W., Jones, C., and Tucker, W. 1985, *Ap. J.*, **293**, 102.
- Gavazzi, G., Perola, G. C., and Jaffe, W. 1981, *Astr. Ap.*, **103**, 35.
- Gilmore, G., and Shaw, M. A. 1986, *Nature*, **321**, 750.
- Golombek, D., Miley, G. K., and Neugebauer, G. 1988, *A. J.*, **95**, 26.
- Grandi, S. A. 1977, *Ap. J.*, **215**, 446.
- Greuff, G., and Vigotti, M. 1973, *Astr. Ap. Suppl.*, **11**, 41.
- Hansen, L., Norgaard-Nielsen, H. U., and Jorgensen, H. E. 1985, *Astr. Ap.*, **149**, 442.
- Harris, A. 1972, *M.N.R.A.S.*, **158**, 1.
- Heckman, T. M. 1981, *Ap. J. (Letters)*, **250**, L59.
- . 1983, *Ap. J. (Letters)*, **271**, L5.
- Heckman, T. M., Baum, S. A., van Breugel, W., and McCarthy, P. 1989, *Ap. J.*, in preparation.
- Heckman, T. M., Miley, G. H., Balick, B., van Breugel, W. J. M., and Bothun, H. R. 1982, *Ap. J.*, **262**, 529.
- Heckman, T. M., Smith, E. P., Baum, S. A., van Breugel, W. J. M., Miley, G. K., Illingworth, G. D., Bothun, G. D., and Balick, B. 1986, *Ap. J.*, **311**, 526 (H86).
- Heckman, T. M., van Breugel, W. J. M., and Miley, G. H. 1984, *Ap. J.*, **286**, 509.
- Hine, R. G., and Longair, M. S. 1979, *M.N.R.A.S.*, **188**, 111.
- Hoessel, J. G., Borne, K. D., and Schneider, D. P. 1985, *Ap. J.*, **293**, 94.
- Hogbom, J. A. 1979, *Astr. Ap. Suppl.*, **36**, 173.
- Hutchings, J. B. 1987, *Ap. J.*, **320**, 122.
- Hu, E. M., Cowie, L. L., and Wang, Z. 1985, *Ap. J. Suppl.*, **59**, 447.
- Isobe, T., Feigelson, E. D., and Nelson, P. I. 1986, *Ap. J.*, **306**, 490.
- Johnstone, R. M., Fabian, A. C., and Nulsen, P. E. J. 1987, *M.N.R.A.S.*, **224**, 75.
- Kapahi, V. K., and Saikia, D. J. 1982, *J. Astr. Ap.*, **3**, 161.
- Kinney, A. L., Huggins, P. J., Bregman, J. N., and Glassgold, A. E. 1985, *Ap. J.*, **291**, 128.
- Koski, A. T. 1978, *Ap. J.*, **223**, 56.
- Kwan, J., and Krolik, J. H. 1981, *Ap. J.*, **250**, 478.
- Laing, R. A., and Bridle, A. H. 1987, preprint.
- Large, M. I., Mills, B. Y., Little, A. G., Crawford, D. F., and Sutton, J. M. 1981, *M.N.R.A.S.*, **194**, 693.
- Lauer, T. 1984, *Ap. J.*, **311**, 34.
- . 1987, preprint.
- Lea, S. M., and Holman, G. D. 1978, *Ap. J.*, **222**, 29.
- Lequeux, J., Peimbert, M., Rayo, J. F., Serrano, A., and Torres-Peimbert, S. 1979, *Astr. Ap.*, **80**, 155.
- Longair, M. S., and Seldner, M. 1979, *M.N.R.A.S.*, **189**, 433.
- McCarthy, P., van Breugel, W., Spinrad, H., and Djorgovski, S. 1987, *Ap. J. (Letters)*, **321**, L29.
- McDonald, G. H., Kenderdine, S., and Neville, A. C. 1968, *M.N.R.A.S.*, **138**, 259.
- Nulsen, P. E. J. 1986, *M.N.R.A.S.*, **221**, 377.

- Nulsen, P. E. J., Steward, G. C., and Fabian, A. C. 1984, *M.N.R.A.S.*, **208**, 185.
 Oort, M. J. A., Katgut, P., Steeman, F. W. M., and Windhorst, R. A. 1987, *Astr. Ap.*, **179**, 41.
 Osterbrock, D. E. 1974, *Astrophysics of Gaseous Nebula* (San Francisco: Freeman).
 Osterbrock, D. E., and Miller, J. S. 1975, *Ap. J.*, **197**, 535.
 Palimaka, J. J., Bridle, A. H., Fomalont, E. B., and Brandie, G. W. 1979, *Ap. J. (Letters)*, **231**, L7.
 Phillips, M. M., Jenkins, C. R., Dopita, M. A., Sadler, E. M., and Binette, L. 1986, *Ap. J.*, **91**, 1062.
 Quinn, P. J. 1984, *Ap. J.*, **279**, 596.
 Rephaeli, Y. 1987, *M.N.R.A.S.*, **225**, 851.
 Robinson, A., Binette, L., Fosbury, R. A. E., and Tadhunter, C. N. 1987, *M.N.R.A.S.*, **227**, 97.
 Sarazin, C. L. 1986, *Rev. Mod. Phys.*, **58**, 1.
 Sarazin, C. L., and White, R. E., III. 1987, *Ap. J.*, **320**, 32.
 Saslaw, W. C., Tyson, J. A., and Crane, P. 1978, *Ap. J.*, **222**, 435.
 Schmidt, M. 1966, *Ap. J.*, **146**, 7.
 Schreier, E. J., Gorenstein, P., and Feigelson, E. D. 1982, *Ap. J.*, **261**, 42.
 Schweizer, F. 1986, *Science*, **231**, 227.
 Smirnov, N. V. 1939, *Bull. Moscow Univ.*, **2(2)**, 3.
 Smith, E. 1988, Ph.D. thesis, University of Maryland.
 Spinrad, H., Djorgovski, S., Marr, J., and Aguilar, L. 1985, *Pub. A.S.P.*, **93**, 932.
 Staff of the Division of Radiophysics, CSIRO. 1969, *Australian J. Phys.*, *Ap. Suppl.*, **7**, 1.
 Stewart, G. C., Fabian, A. C., Jones, C., and Forman, W. 1984, *Ap. J.*, **285**, 1.
 Stockton, A., and MacKenty, J. W. 1987, *Ap. J.*, **316**, 584.
 Thomas, P. A., Fabian, A. C., Arnaud, K. A., Forman, W., and Jones, C. 1986, *M.N.R.A.S.*, **222**, 655.
 Toomre, A. 1977, in *Evolution of Galaxies and Stellar Populations*, ed. B. M. Tinsely and R. B. Larson (New Haven: Yale University Observatory), p. 401.
 Toomre, A., and Toomre, J. 1972, *Ap. J.*, **178**, 623.
 Tubbs, A. D. 1980, *Ap. J.*, **241**, 969.
 Tucker, W. H., and Rosner, R. 1983, *Ap. J.*, **267**, 547.
 Ulrich, M.-H., and Meier, D. L. 1984, *A.J.*, **89**, 203.
 van Albada, T. S., Kotanyi, C. G., and Schwarzschild, M. 1982, *M.N.R.A.S.*, **198**, 303.
 van der Hulst, J. M., Golisch, W. F., and Haschick, A. D., 1983, *Ap. J. (Letters)*, **264**, L37.
 White, R. E., III, and Chevalier, R. A. 1984, *Ap. J.*, **280**, 561.
 Whitford, A. E. 1958, *A.J.*, **63**, 201.
 ———. 1975, in *Galaxies and the Universe*, ed. A. Sandage, M. Sandage, and R. Kristian (Chicago: University of Chicago Press), p. 159.
 Whittle, M. 1985, *M.N.R.A.S.*, **213**, 33.
 Wills, B. J. 1975, *Australian J. Phys.*, *Ap. Suppl.*, **38**, 1.
 Wilkinson, A., Hine, R. G., and Sargent, W. L. W. 1981, *M.N.R.A.S.*, **196**, 669.
 Yee, H. K. C., and Oke, J. B. 1978, *Ap. J.*, **226**, 753.
 Zanstra, H. 1931, *Pub. Dom. Ap. Obs.*, **4**, 209.

STEFI ALISON BAUM: Radiosterrenwacht, Postbus 2, 7990 AA, Dwingeloo, The Netherlands

TIMOTHY M. HECKMAN: Astronomy Program, University of Maryland, College Park, MD 20742